Investigation of the Host Kinome Response to Coronavirus Infection Reveals PI3K/mTOR Inhibitors as Betacoronavirus Antivirals

Ethan J. Fritch, Angie L. Mordant, Thomas S.K. Gilbert, Carrow I. Wells, Xuan Yang, Natalie K. Barker, Emily A. Madden, Kenneth H. Dinnon, III, Yixuan J. Hou, Longping V. Tse, Izabella N. Castillo, Amy C. Sims, Nathaniel J. Moorman, Premkumar Lakshmanane, Timothy M. Willson, Laura E. Herring, Lee M. Graves, and Ralph S. Baric*

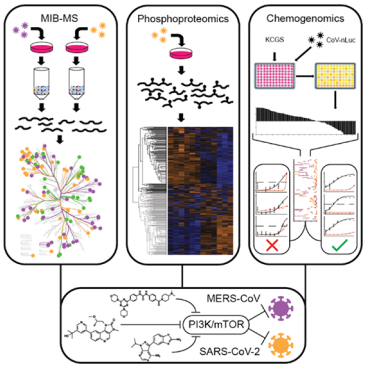

ABSTRACT: Host kinases play essential roles in the host cell cycle, innate immune signaling, the stress response to viral infection, and inflammation. Previous work has demonstrated that coronaviruses specifically target kinase cascades to subvert host cell responses to infection and rely upon host kinase activity to phosphorylate viral proteins to enhance replication. Given the number of kinase inhibitors that are already FDA approved to treat cancers, fibrosis, and other human disease, they represent an attractive class of compounds to repurpose for host-targeted therapies against emerging coronavirus infections. To further understand the host kinome response to betacoronavirus infection, we employed multiplex inhibitory bead mass spectrometry (MIB-MS) following MERS-CoV and SARS-CoV-2 infection of human lung epithelial cell lines. Our MIB-MS analyses revealed activation of mTOR and MAPK signaling following MERS-CoV and SARS-CoV-2 infection, respectively. SARS-CoV-2 host kinome responses were further characterized using paired phosphoproteomics, which identified activation of MAPK, PI3K, and mTOR signaling. Through chemogenomic screening, we found that clinically relevant PI3K/mTOR inhibitors were able to inhibit coronavirus replication at nanomolar concentrations similar to direct-acting antivirals. This study lays the groundwork for identifying broad-acting, host-targeted therapies to reduce betacoronavirus replication that can be rapidly repurposed during future outbreaks and epidemics. The proteomics, phosphoproteomics, and MIB-MS datasets generated in this study are available in the Proteomics Identification Database (PRIDE) repository under project identifiers PXD040897 and PXD040901.

KEYWORDS: *SARS-CoV-2, MERS-CoV, phosphoproteomics, MIB-MS, kinase inhibitors, kinome*

INTRODUCTION

Coronaviruses (CoVs) commonly cause cold-like symptoms and lower respiratory tract infections in humans and are agricultural pathogens of concern for multiple livestock species.[3−5] Over the past 20 years, three highly pathogenic CoVs have emerged from animal reservoirs to cause human disease; severe acute respiratory syndrome coronavirus (SARS-CoV), Middle East respiratory syndrome coronavirus (MERS-CoV), and severe acute respiratory syndrome coronavirus 2 (SARS-CoV-2).[6−8] SARS-CoV was controlled through public health intervention strategies that limited human transmission, but MERS-CoV remains endemic in camels in northern Africa and the Arabian Peninsula, causing a low number of human cases annually.[9,10] SARS-CoV-2 has shown the true pandemic potential of CoVs, causing about 760 million cases of COVID-19 worldwide, ∼6.9 million of which resulted in death.[11] While deployment of multiple vaccine platforms has managed to curb the severe disease incidence of COVID-19, antigenic variation has led to persistence of SARS-CoV-2 spread and continued mortality.[12,13] COVID-19 survivors may also experience long COVID in the presence and absence of virus infection, resulting in neurologic, pulmonary, cardiac, and renal complications, dictating a need to identify and target conserved host signaling pathways that function in acute and chronic disease.[14,15] Moreover, a wealth of zoonotic CoVs display a broad host range and the capacity to use human receptors for entry in primary cells, and development of further therapeutic options will be necessary to reduce viral replication and disease burden against contemporary, emerging, and future CoV disease.[16−19]

Since the beginning of the COVID-19 pandemic, numerous studies focused on potential drug repurposing, either for existing small molecules that may bind CoV proteins or for the

Received: March 29, 2023

specific targeting of host pathways for reduction of viral replication.[20−24] A number of these papers describe attempts to identify host kinase responses to SARS-CoV-2 infection and to then target these kinases with preexisting inhibitors to reduce viral replication.[25−28] While kinase inhibitors have been developed as cancer therapeutics due to the central role of kinases in regulating cellular proliferation and death, immune responses, and intracellular signaling,[29] their effects on viral replication are less well understood. CoVs specifically target antiviral kinase cascades to circumvent innate immunity and alter host cells to create optimal environments for replication of progeny.[30] Moreover, several CoV proteins are phosphorylated by host kinases following infection, suggesting that some host kinase activity can result in pro or antiviral activity as well.[31−33] The number of kinase inhibitors that are clinically approved or have clinical trial data represents a large pool for rapid drug repurposing, making them a desirable set to study.[34,35]

Furthermore, we had a specific interest in determining if there are similar kinase activity signatures across the two circulating highly pathogenic CoVs, MERS-CoV, and SARS-CoV-2. To investigate this, we performed multiplex inhibitor bead mass spectrometry (MIB-MS) analysis on both MERS-CoV- and SARS-CoV-2-infected cells. We performed parallel phosphoproteomics from SARS-CoV-2-infected cells to obtain a more complete picture of the kinase landscape during SARS-CoV-2 infection through compared analysis of MIB-MS and phosphoproteomics. Last, we completed an untargeted chemogenomic inhibitor screen to identify kinases and pathways that may serve as druggable targets. A library of clinically relevant kinase inhibitors was then prepared from analysis of proteomic and chemogenomic datasets and screened in both CoV systems. Our data indicate that disruption of kinase activity can decrease CoV viral replication and that there is potential drug repurposing of kinase inhibitors as antivirals. Most importantly, we identified distinct and shared pathways affected by MERS-CoV and SARS-CoV-2 infection, with the PI3K/mTOR pathway as a candidate target for broad-acting betacoronavirus growth inhibition.

EXPERIMENTAL PROCEDURES

Collection of MERS-CoV-Infected Cells

Calu-3 cells, a human airway epithelial cell line, were plated 3 days prior to infection at 3×10^7 cells per flask.[36] Immediately prior to infection, icMERS-CoV stocks were diluted in PBS for a final multiplicity of infection (MOI) of 3 in 3 mL of inoculum.[37] Cell growth media were removed from all flasks, and cells were washed once with PBS (Gibco). Inoculum or PBS was added to the monolayers, and flasks were rocked every 15 min for 1 h. Inoculum was removed, and flasks were washed once with PBS prior to addition of viral growth medium, MEM (Gibco) supplemented with heat-inactivated fetal bovine serum (HyClone). At 4, 12, and 24 h post infection, viral growth media were removed, an aliquot was reserved for titer, and cells were washed once with PBS prior to scraping the monolayer in fresh PBS from the surface of the flask. Cells were concentrated by low-speed centrifugation, supernatant was removed, and pellets were flash frozen with dry ice and then placed at −80 °C until further processing. Infected samples were collected in triplicate at each timepoint with one mock sample collected at each timepoint.

Collection of SARS-CoV-2-Infected Cells

As SARS-CoV-2 replicates less efficiently than MERS-CoV in Calu3 cells, A549 cells, isolated from the lung tissue of a 58-year-old Caucasian male, expressing hACE2 (A549-hACE2) were plated 3 days prior to infection for confluency.[38] One day prior to infection, cell growth media were removed, monolayers were washed, and cells were given low serum media. Immediately prior to infection, icSARS-CoV-2 stocks were diluted in PBS for a final MOI of 3 in 3 mL of inoculum.[39] Cell growth media were removed from all flasks, and cells were washed once with PBS (Gibco). Inoculum or PBS was added to the monolayers, and flasks were rocked every 15 min for 1 h. Inoculum was removed and flasks were washed once with PBS prior to addition of viral growth medium, and MEM (Gibco) was supplemented with heat-inactivated fetal bovine serum (HyClone). At 4, 12, and 24 h post infection, viral growth media were removed, an aliquot was reserved for titer, and cells were washed once with PBS prior to scraping the monolayer in fresh PBS from the surface of the flask. Cells were spun down, supernatant was removed, and pellets were flash frozen with dry ice then placed at −80 °C until further processing. Infected samples were collected in triplicate at each timepoint with one mock sample collected at each timepoint.

Cell Lysis and MIB Column Kinase Capture

Infected and mock cell pellets were thawed on ice, resuspended in lysis buffer containing protease inhibitor cocktail (Roche) and Phosphatase Inhibitor Cocktails 2 and 3 (Sigma-Aldrich) as previously described, and placed into 2 mL tubes containing 0.1 mm zirconium beads (Sigma-Aldrich).[1] Lysates were then agitated for 1 min using a Beadbeater-16 (BioSpec Products) and centrifuged, and supernatant was removed from beads to be clarified through 0.22 μM syringe filters. Protein in lysates was quantified via BCA assay (Pierce), and equal amounts of protein from each sample were brought.

Lysates were added to equilibrated MIB capture columns containing a 400 μL slurry of equal parts, ECH Sepharose conjugated PP58, Purvalanol B, UNC-2147A, and VI-16832 beads.[1] 2.6 mg of protein was loaded for MERS-CoV samples, and 3 mg of protein was loaded for SARS-CoV-2 samples. The columns were washed first with high salt buffer containing 1 M NaCl, 50 mM HEPES, 0.5% Triton X-100, 1 mM EDTA, and 1 mM EGTA, and then with low salt buffer containing the same formulation with 150 mM NaCl instead, and finally with low salt buffer supplemented with 0.1% SDS. Captured kinases were eluted in SDS elution buffer supplemented with 1% β-mercaptoethanol by boiling for 10 min. Eluates were reduced (5 mM DTT, 30 min, 60 °C) (Sigma) and alkylated (10 mM iodoacetic acid, 30 min, RT) (Sigma), before being concentrated 10× (Millipore). Protein was extracted from the concentrate by methanol-chloroform precipitation and then digested overnight with trypsin (Promega). Digested peptides were further cleaned with ethyl acetate extraction and desalted using C18 spin columns (Pierce), as previously described.[1]

MIBS samples were analyzed by nLC−MS/MS using an Easy nLC 1200 coupled to a Q Exactive HF mass spectrometer (Thermo). Samples were injected onto an EASY-Spray PepMap C18 column (75 μm id × 25 cm, 2 μm particle size) (Thermo Scientific) and separated over a 120 min method. The gradient for separation consisted of 5−38% mobile phase B at a 250 nL/min flow rate, where mobile phase

A was 0.1% formic acid in water and mobile phase B consisted of 0.1% formic acid in 80% acetonitrile. The Q Exactive HF was operated in data-dependent mode where the 15 most intense precursors were selected for subsequent fragmentation. The resolution for the precursor scan (m/z 350−2000) was set to 120,000 with a target value of 3×10^6 ions. The MS/MS scan resolution was set to 15,000 with a target value of 1×10^5 ions, 100 ms max IT. The normalized collision energy was set to 27% for high-energy collision dissociation. Dynamic exclusion was set to 30 s, and precursors with unknown charge or a charge state of 1 and ≥8 were excluded.[40]

Sample Preparation and nLC-MS/MS for Proteomics/Phosphoproteomics Analysis

Aliquots of SARS-CoV-2 lysates (n = 3) that were prepared prior to MIB columns were placed at −80 °C immediately after lysis. These aliquots were later thawed, and 500 μg of protein from each sample was precipitated via methanol-chloroform precipitation. Protein pellets were washed twice with methanol prior to reconstitution in 8 M urea in 50 mM Tris−HCl (Sigma-Aldrich). Protein samples were reduced with 5 mM DTT for 30 min, alkylated with iodoacetamide in the dark at room temperature for 45 min, and then digested with LysC for 2 h at 37 °C, followed by an overnight trypsin digestion at 37 °C (1:50 protease:protein ratio). Resulting peptides were desalted using C18 desalting columns (Pierce), and then peptide quantitation was conducted using BCA peptide fluorometric assay (Pierce). Each sample (200 μg) was aliquoted, and a pooled sample was created by combining 70 μg of each sample. This pooled sample was subsequently divided into four different pooled aliquots. Samples were subsequently labeled with 400 μg of TMTpro 16plex reagents (Thermo) for 1 h at 25 °C. Prior to quenching, labeling efficiency (>98%) was verified by nLC−MS/MS analysis. Upon verification, samples were quenched, mixed 1:1, cleaned via C18 desalting columns (Pierce), and dried down via vacuum centrifugation and then stored at −80 °C until further processing.

The TMT-labeled sample was subjected to off-line HPLC fractionation (Agilent 1260 System) using high-pH reversed-phase chromatography to generate 24 fractions, of which 5% of each fraction was aliquoted and dried down via vacuum centrifugation for proteome analysis.[41] The remaining 95% of each fraction was pooled down to four fractions, which were enriched for phosphopeptides using High Select FeNTA (Thermo). Eluates were dried down via vacuum centrifugation for phosphoproteome analysis. Each proteome and phosphoproteome fraction (28 in total) were analyzed by LC-MS/MS using an Easy nLC 1200 coupled to an Orbitrap Fusion Lumos mass spectrometer (Thermo). Samples were injected onto an EASY-Spray PepMap C18 column (75 μm id × 25 cm, 2 μm particle size) (Thermo Scientific) and separated over a 120 min method. The gradient for separation consisted of 5−42% mobile phase B at a 250 nL/min flow rate, where mobile phase A was 0.1% formic acid in water and mobile phase B consisted of 0.1% formic acid in 80% acetonitrile.

For the proteome fractions, the Lumos was operated in SPS-MS3 mode with a 3 s cycle time.[42] The resolution for the precursor scan (m/z 400−1500) was set to 120,000 with an automatic gain control target set to standard and a maximum injection time of 50 ms. MS2 scans consisted of collision-induced dissociation normalized collision energy (NCE) of 32; an AGC target set to standard; a maximum injection time of 50 ms; and an isolation window of 0.7 Da. Following MS2 acquisition, MS3 spectra were collected in synchronous precursor selection mode (10 scans per outcome), with an HCD set to 55; a resolution set to 50,000; a scan range set to 100−500; and an AGC target set to 200% with a 100 ms maximum inject time.

For the phosphoproteome fractions, the Lumos was operated in MS2 mode with a 3 s cycle time.[26,43] The resolution for the precursor scan (m/z 400−1500) was set to 60,000 with an AGC target set to standard and a maximum injection time of 50 ms. For MS2 scans, the HCD was set to 35; the AGC target set to 200%; the maximum injection time was 120 ms; the isolation window was 0.7 Da; and the resolution was set to 50,000.

Data Analysis of the MIB-MS Data

For the kinome data, all raw files were processed using MaxQuant (version 1.6.15.0) and searched against the reviewed human database (containing 20,350 entries, downloaded February 2020), appended with the Sars-CoV-2 database (containing 15 entries, downloaded September 2020) and a contaminants database. Enzyme specificity was set to trypsin, and up to two missed cleavage sites were allowed. For modifications, cysteine carbamidomethylation was set as a fixed modification while methionine oxidation and protein N-terminus acetylation were set as variable modifications. A 1% peptide/protein FDR was used to filter all data. Match between runs was enabled (0.7 min match time window, 20 min alignment window), and a minimum of one peptide was required for label-free quantitation (LFQ) using the LFQ intensities.

Perseus (version 1.6.14.0) was used for further processing.[44] Kinases were parsed, and only kinases with >1 unique+razor peptide were used for LFQ analysis. Kinases with 50% missing values were removed, and missing values were imputed. Log2 fold change ratios were calculated using the averaged Log2 LFQ intensities, and Student's t-test was performed for each pair-wise comparison. Kinases with p-value <0.05 and Log2 fold change (FC) ratio ± 0.5 were considered significant.

Data Analysis of the Proteome/Phosphoproteomics Data

For the proteome and phosphoproteome data, all raw files were processed using Proteome Discoverer version 2.5. "TMTpro 16plex" was used as the quantitation method. Peak lists were searched against a reviewed UniProt human database (downloaded Feb 2020 containing 20,350 sequences), appended with a common contaminants database, using Sequest HT within Proteome Discoverer. Data were searched with up to two missed trypsin cleavage sites, and fixed modifications were set to TMTpro peptide N-terminus and Lys and carbamidomethyl Cys. Dynamic modifications were set to N-terminal protein acetyl and oxidation Met.

For phosphoproteome data, additional dynamic modification was set to phosphorylation Ser, Thr, and Tyr. TMT quantitation was set to MS2, precursor mass tolerance was set to 10 ppm, and fragment mass tolerance was set to 0.02 Da. The peptide false discovery rate was set to 1%. The ptmRS node was used to localize phosphorylation sites within peptides. Reporter abundance based on intensity and co-isolation threshold was set to 50.

For proteome data, quantitation was set to MS3, precursor mass tolerance was set to 10 ppm, and fragment mass tolerance was set to 0.5 Da. The peptide false discovery rate was set to 1%. Reporter abundance based on intensity, SPS mass match

threshold set to 50, and razor and unique peptides were used for quantitation. The phosphoproteome dataset was imported into RStudio (v. 4.1.1), and redundant phosphosites on peptides with differing charge states were collapsed to one value representing the mean of LFQ abundances per sample using the doBy package.[45] The curated phosphoproteomics dataset, as well as the proteomics dataset, was then imported into Perseus (version 1.6.14.0), where normalized TMT intensities of the phosphopeptides and proteins were log2 transformed and missing values were imputed from a normal distribution (width 0.3 and downshift of 1.8); then, log2 fold change ratios and Student's t-test *p*-values were calculated for each pairwise comparison.[44]

For hierarchical clustering (based on Euclidean distance and average linkage), log2 TMT intensities were *z*-score normalized and the relative abundance changes of these phosphopeptides between the infected and the mock samples were visualized. Phosphopeptides were clustered based on their relative abundance over time (i.e., formed an abundance gradient across the 4−12−24 hpi time points). The phosphopeptides and corresponding abundance values were exported from Perseus into two datasets respective of their clusters: cluster I. "DOWN" means phosphopeptides that decreased in abundance compared to the mock and over time; II. "UP" means phosphopeptides that increased in abundance compared to the mock and over time. These two datasets ("UP" and "DOWN" clusters) were then uploaded into Ingenuity Pathway Analysis (Qiagen, 2022) with the following cutoffs: *p*-value <0.05 and Log2 FC >0.5 or <−0.5, in the 24 hpi/mock comparison.[46] The Canonical Signaling pathways affected by the phosphorylated proteins were manually curated to retain only the significantly overrepresented (*p*-value <0.05) and significantly activated (*z*-score >2) or inhibited (*z*-score <−2) pathways of relevance. A graphic of selected pathways was generated in RStudio (v. 4.2.0) with the tidyverse package and enhanced in Adobe Illustrator (2022).[47] A graphic representing the phosphorylated proteins from cluster II (24 hpi/mock comparison) involved in the mTOR signaling pathway was generated by directly exporting the figure from IPA.

Individual Inhibitory Bead Pulldowns of Nucleocapsid

Purified mannose-binding protein (MBP)-fused SARS-CoV-2 nucleocapsid was produced as previously described.[48] 20 μg of purified protein, individual inhibitor beads, blank beads, and MIB mix were individually equilibrated in high salt buffer identical to that used for MIB-MS. Equilibrated proteins and beads were mixed and incubated while rotating for 2 h at 4 °C. Following incubation, beads were pelleted via centrifugation, supernatant removed, and washed with high salt buffer for 2 min at 25 °C while rotating. This step was then repeated with low salt buffer and low salt buffer containing 0.1% SDS to mimic washes used for MIB-MS. Following removal of low salt buffer containing 0.1% SDS, the bound protein was eluted from beads via heating at 95 °C in 1× Laemmli (Bio-Rad) in low salt buffer containing 0.1% SDS and 2.5% β-mercaptoethanol (Sigma).

SDS-PAGE and Western Blot

Eluates from pulldowns were loaded into 4−20% gradient mini-gels (Bio-Rad) for SDS-PAGE. Proteins were transferred from the mini-gel onto a PVDF membrane (Pierce) using a semi-dry transfer apparatus (Bio-Rad) and blocked using 5% non-fat dry milk in 1× Tris-buffered saline (Sigma) supplemented with 0.1% Tween-20 (TBS-T) (Sigma). A primary anti-MBP antibody (Sigma M1321) was diluted to 0.1 μg/mL in block, and membranes were incubated overnight at 4 °C. Membranes were washed three times using TBS-T prior to incubation with secondary sheep anti-mouse HRP (Amersham ECL) in block for 1 h at 25 °C. Membranes were washed three times prior to addition of SuperSignal Pico PLUS (Fisher) and imaging via iBright FL1500 (Fisher).

Luciferase-Based Growth Inhibition Screen

Calu3 or A549-hACE2 cells were plated 1 day prior to infection for confluency in 96-well clear-bottom black plates (Corning). A kinase inhibitor library was prepared from the kinase chemogenomic set (KCGS) of 187 compounds targeting 215 host kinases and inhibitors of kinases implicated in MERS-CoV replication from MIB-MS (ID3).[49] On the day of infection, drug stocks suspended in DMSO at 10 mM were diluted to 1 mM in DMSO and then diluted 1:100 in infection media of DMEM (Gibco) supplemented with heat-inactivated fetal bovine serum (HyClone). Cell growth media were aspirated from plates and replaced with diluted drug in media. Cell growth media were removed from 96-well plates, and 50 μL of drug dilution was added to pretreat the cells. MERS-CoV nLuc or SARS-CoV-2 nLuc stock was diluted for a final MOI of 0.02 in 50 μL of viral growth media.[50,51]

Viral inoculum or mock inoculum containing just viral growth media was added to cells 1 h post drug treatment 1:1 for a final concentration of drug treatment of 5 μM. Plates were incubated for 2 days at 37 °C. Virus-infected plates were subjected to Nano-Glo reagent (Promega) while mock-infected plates were subjected to CellTiter-Glo 2.0 reagent (Promega) according to the manufacturer's instructions. Luminescence readings for MERS-CoV KCGS and ID3 screens were taken on a SpectraMax (Molecular Devices) while SARS-CoV-2 KCGS screen readings were taken on a GloMax plate reader (Promega); data was exported for analysis in Excel. Wells without cells were included to account for background nano-luciferase signal, cells with DMSO-only treatment were included to normalize the luminescence signal, and remdesivir was included as a control on each plate.

Drug Selection for Clinical Kinase Screen

To maximize the opportunity for drug repurposing during the COVID-19 pandemic, we assembled a clinical kinase screen (CKS) based upon compounds that had advanced to clinical trials or had been approved as drugs by the FDA.[35,52] The combined chemoproteomic and chemogenomic datasets implicated 135 host kinases for their potential involvement in replication of a β-coronavirus (Supplemental Data 6). Multiple databases were searched to identify the clinically advanced kinase inhibitors that were reported to inhibit one or more of the kinases as either a primary or collateral target. Whenever possible, more than one kinase inhibitor was selected for each host kinase to increase confidence that viral inhibition was associated with a specific kinase target. In total, 93 kinase inhibitors were assembled for the CKS, of which 87 had already been dosed in humans.

Luciferase-Based Dose−Response Curves

Calu3 or A549-hACE2 cells were plated 1 day prior to infection for confluency in 96-well clear-bottom black plates (Corning). On the day of infection, drug stocks suspended in DMSO at 10 mM were diluted to 2 mM in DMSO (Sigma-Aldrich). 2 mM aliquots of drug were serially diluted in DMSO

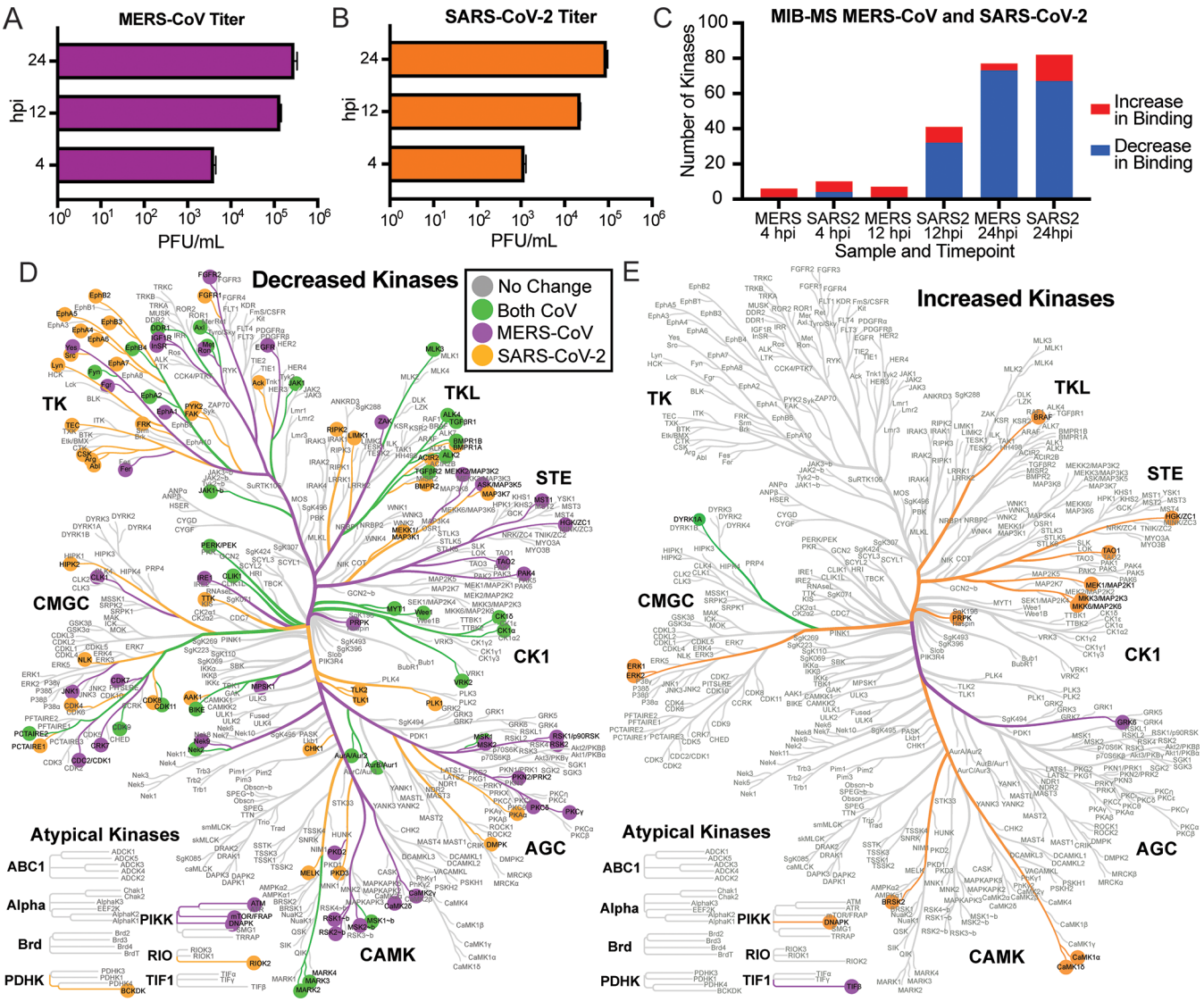

Figure 1. Kinases differentially bind to MIBs following CoV infection. Human airway epithelial cells were infected with MERS-CoV and SARS-CoV-2 at an MOI of 3. Cells were collected at 4, 12, and 24 hpi, lysed, and ran over MIB columns to capture kinases. MIB columns were washed, kinases were eluted and prepared for mass spectrometry, and changes in kinase abundance were compared to mock-infected MIB samples. (A) MERS-CoV titer of infected Calu3 cells at MIB-MS collection timepoints. (B) SARS-CoV-2 titer of infected A549-hACE2 cells at MIB-MS collection timepoints. (C) Number of differentially binding kinases in both CoV infections throughout infection compared to mock (p-value <0.05). Red indicates a Log2 fold increase >0.5, and blue indicates a Log2 fold decrease <−0.5 (C). Visualization of kinases with (D) decreased or (E) increased binding at 24 h post CoV infection. Gray indicates no significant change compared to mock, green indicates similar change following both MERS-CoV and SARS-CoV-2 infection, purple indicates change only in MERS-CoV infection, and orange indicates change only in SARS-CoV-2 infection (D, E). Mean and standard error of the mean calculated in Prism 9 (A, B). Graphs created in Prism 9 (A–C). Kinase trees created in Coral and enhanced in Adobe Illustrator (D, E).[2]

fourfold for an eight-point dilution curve. Serial dilutions were further diluted 1:100 in infection media of DMEM (Gibco) supplemented with FetalClone II (HyClone), non-essential amino acids (Gibco), and Pen-Strep (Gibco). Cell growth media were removed from 96-well plates, and 50 μL of drug dilution was added to pretreat the cells. MERS-CoV or SARS-CoV-2 nLuc stock was diluted for a final MOI of 0.02 in 50 μL of viral growth media. Viral inoculum or mock inoculum was added to cells 1 h post drug treatment 1:1 for a final concentration at the top of the dose–response curves of 10 μM. Plates were incubated for 2 days at 37 °C. Virus-infected plates were subjected to Nano-Glo reagent (Promega) while mock-infected plates were subjected to Multi-Tox-Glo reagent (Promega) according to the manufacturer's instructions. Luminescence readings were taken on a GloMax plate reader (Promega), and data was exported for analysis in Excel. Wells without cells were included to account for background nano-luciferase signal, and cells with DMSO-only treatment were included to normalize the luminescence signal on each plate. A single dose of remdesivir at 5 μM was included as a positive control for growth inhibition, and staurosporine at 5 μM was included as a positive control for cytotoxicity on each plate. A remdesivir dose–response curve was included in each biological replicate as a control.

Luciferase Assay Data Analysis

Dose–response curves were completed in technical replicate and biological triplicate. The average background signal was

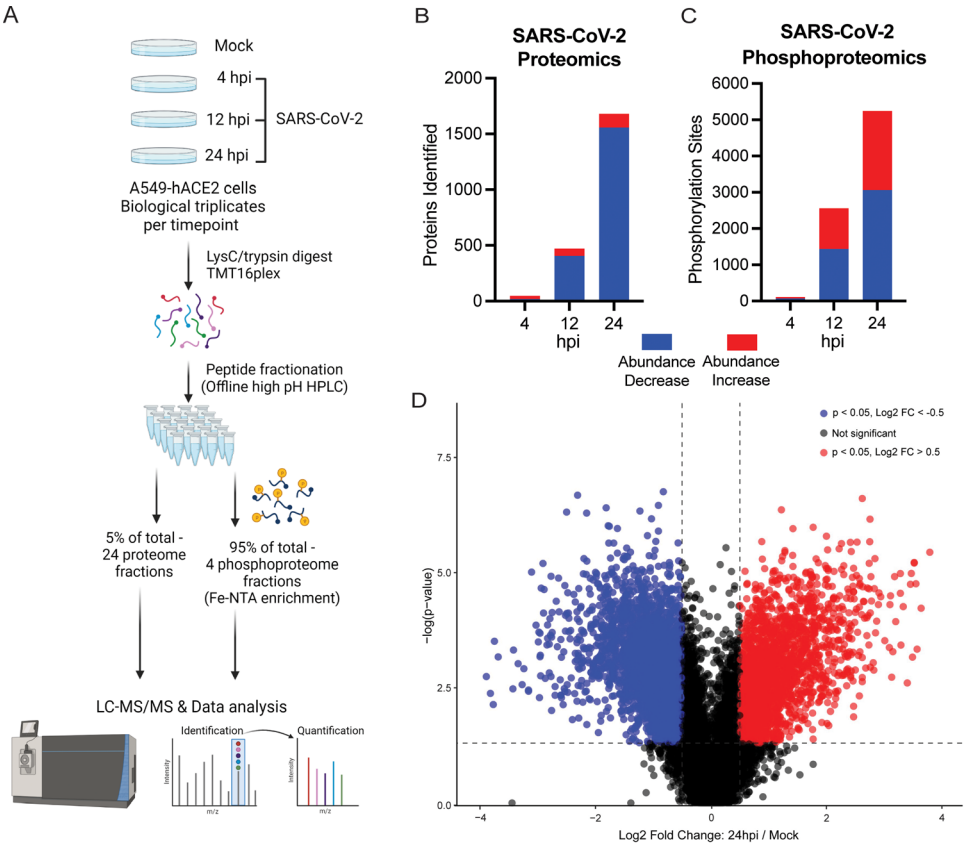

Figure 2. Phosphoproteomic and proteomic analysis of SARS-CoV-2 infection reveals balanced increase in changing phosphorylation sites in the presence of decreasing protein abundance. (A) Aliquots of A549-hACE2 lysate collected for MIB-MS analysis of SARS-CoV-2 infection were processed for proteomic and phosphoproteomic profiling. (B) Proteins and (C) phosphosites with statistically significant changes (p-value <0.05; log2 FC ±0.5) in abundance compared to mock following SARS-CoV-2 infection. Red indicates increase in abundance, and blue indicates decrease in abundance (B, C). (D) Volcano plots of phosphosite changes at 24 hpi. Gray indicates no statistical and/or biological significance compared to mock by p-value >0.05 and/or Log2 fold change not meeting the threshold of ±0.5. Blue indicates statistically significant difference to mock and decrease in phosphosite abundance by Log2 FC <−0.5, and red indicates statistically significant difference to mock and increase in phosphosite abundance by Log2 FC > 0.5. Workflow figure was created in BioRender (A). Data graphed in Prism 9 (B, C) and RStudio (v 4.2.0) using the ggplot2 package (D), and enhanced in Adobe Illustrator (2022).

calculated per plate using wells without cells that were inoculated with virus or mock inoculum and subtracted from all treated wells on the plate. The average positive signal representing 0% growth inhibition for virus-infected plates was calculated from background-corrected wells treated with DMSO per plate. The average positive signal representing 100% cytotoxicity was calculated from background-corrected wells treated with staurosporine (Sigma-Aldrich). The background-corrected signal from wells treated with drug was normalized to average positive signal calculated per plate and used to determine the percent inhibition of viral growth or percent cytotoxicity. Data was imported into Prism 9 to calculate and graph the average, the standard error of the mean, and the non-linear curves fit for IC50 and CC50 values.

RESULTS

Kinome Profiling Using MIB-MS Reveals Differential Host Kinome Response to CoV Infection

Using cell culture models with similar replication kinetics and final titers (Figure 1a,b), MERS-CoV and mock-infected Calu3 cells or SARS-CoV-2 and mock-infected A549-ACE2 cells were collected over a 24 h infection time course. Biological triplicates of each cell line were mock-infected, or infected with MERS-CoV or SARS-CoV-2 for 4, 12, and 24 h, and then MIB-MS analysis was performed to identify host kinome changes post-infection. Over 200 kinases were identified over both of the infection time courses, as well as several viral proteins. Principal component analysis demonstrated that the biological replicates were uniquely grouped and distinct from mock samples, with 4 h post infection (hpi) most similar to mock controls (Figure S1). Changes in host kinome response were further reflected by a gradually increasing number of kinases with statistically significant differences (p-value <0.05; log2 FC ±0.5) in binding to MIB columns as compared to mock over the infection time courses of both viruses (Figure 1c). Although a small number of kinases displayed a significant increase in MIB binding early in the time courses (4 hpi), most kinases displayed a significant decrease in MIB binding by the end of the CoV time courses (24 hpi). A delay in kinome response to MERS-CoV infection was seen compared to SARS-CoV-2. SARS-CoV-2 infection showed a stepwise increase in the number of kinases with decreased binding at 12 h, whereas MERS-CoV infection showed little difference in kinase binding compared to mock until 24 hpi (Figure 1c). Kinase binding to MIB was dependent upon both abundance and activity, suggesting that SARS-CoV-2 affects upon the host kinome, which is more dynamic earlier in infection compared to MERS-CoV.

MERS-CoV and SARS-CoV-2 Infections Reveal Distinct and Overlapping Kinome Profiles

Comparison of MERS-CoV and SARS-CoV-2 MIB-MS data at 4 and 12 hpi showed minimal overlap in kinase binding (Supplemental Data 1 and 2). At 4 hpi, the only shared kinase with increased binding to MIBs was PIP5K1A, a key kinase for upstream production of substrate for PI3K/Akt signaling (Figure S2).[53] At 12 hpi, the only shared kinase with altered binding to MIB was deoxycytidine kinase (DCK); however, its binding either decreased or increased in the MERS-CoV and SARS-CoV-2 datasets, respectively (Figure S2). DCK activity may be indicative of replicative stress on the host cell induced by CoV infection, as it plays an important role in the DNA damage response.[54] We were most interested in kinases with increased MIB binding for potential downstream targeting with inhibitors. Notably, CSNK1E and mTOR were kinases with the highest MIB-MS abundance in the MERS-CoV dataset at 4 and 12 hpi, respectively, while in the SARS-CoV-2 MIB-MS dataset, PIP5K1A at 4 hpi and BRSK2 at 12 hpi were the kinases with the highest abundance (Figure S2, Supplemental Data 1 and 2).

By 24 hpi, we observed a large decrease in MIB binding and a significant overlap between the two datasets (Figure 1d). Most notably, there were shared decreases in both the casein kinase and tyrosine kinase-like families, which play essential roles in signal transduction and cell signaling. Both viruses induced decreases in ephrin and SRC-family kinases, suggesting a broad decrease in both receptor and non-receptor tyrosine kinases following CoV infection. There were fewer kinases with increased MIB binding at 24 hpi in both CoV datasets and only one kinase with shared activity at this time point, DYRK1a, which was the most abundant kinase identified at 24 hpi in the MERS-CoV dataset (Figure 1e). DYRK1a is involved in the response to double-stranded DNA breaks, so it may reflect increased apoptosis or cellular stress at the later timepoint.[55] Kinases with increased MIB binding at 24 hpi in the SARS-CoV-2 dataset were mostly involved in MAPK signaling, indicative of activation of stress response to viral infection, while those with increased binding in the MERS-CoV dataset do not appear to converge on any one pathway.

Inferred Kinase Activity from Phosphoproteomics Analysis of SARS-CoV-2 Infection Reveals Activation of Pro-Inflammatory Response and Specific Kinase Pathways

To determine signaling pathways altered over the SARS-CoV-2 time course, global quantitative phosphoproteomic and proteomic analysis of SARS-CoV-2-infected A549-hACE2 was performed on paired cell lysates (n = 3) from the MIB-MS analysis (Figure 2a). Over 7200 proteins and 14,300 phosphosites were quantified over the 24 h infection time course (Supplemental Data 3 and 4). Principal component analysis of the phosphoproteomic data from SARS-CoV-2-infected cells indicated similar grouping as our MIB-MS data, with 4 hpi samples most proximal to mock and the largest separation seen with the 24 hpi samples (Figure S3). Total protein abundance decreased throughout the time course of infection, which follows the known activity of CoV nsp1 to shut down host translation (Figure 2b).[56,57] Although the majority of significantly altered proteins (p-value <0.05; Log2 FC ±0.5) displayed a decrease in abundance over the infection time course, thousands of phosphorylation sites significantly increased by 24 hpi (Figure 2c,d, Figure S3), similar to previous studies.[26,58]

To further characterize the changes in the phosphorylation landscape following SARS-CoV-2 infection, we performed hierarchical clustering of the phosphoproteomics dataset, which revealed two distinct clusters (Figure 3a). Cluster I consisted of phosphosites that had decreased phosphorylation

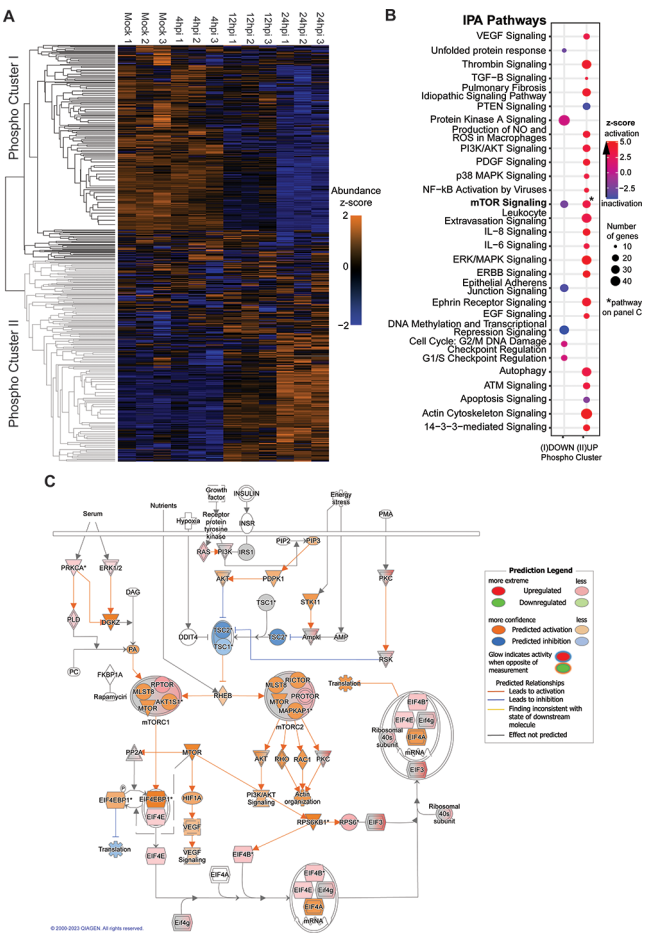

Figure 3. Pathway analysis of phosphoproteomics following SARS-CoV-2 infection reveals specific activation of kinase pathways and mTOR. (A) Hierarchical clustering analysis (Euclidean distance; average linkage) of z-score-normalized Log2 abundance values of phosphopeptides. Phosphopeptides clustered by abundance changes overtime, separating into two distinct clusters: (I) "DOWN" cluster = phosphopeptides that decreased in abundance compared to the Mock and overtime and (II) "UP" = phosphopeptides that increased in abundance compared to the mock and overtime. Orange indicates increased abundance, while purple indicates decreased abundance. (B) Significantly overrepresented IPA canonical pathways (p-value <0.05) that were either activated (z-score > 2) or inhibited (z-score < −2) in phospho clusters I ("DOWN") and II ("UP") from (A). Red indicates activation while blue indicates inhibition measurement by z-score; the size of the bubbles indicates the number of genes included in the pathway that had one or multiple phosphorylation(s) in the dataset (filtered for Log2FC ± 0.5; p-value <0.05). (C) mTOR signaling pathway, which was significantly overrepresented and activated in the 24 hpi samples compared to the mock. Shapes indicate the molecular class of the proteins. Orange indicates predicted protein activation, and blue indicates predicted protein inhibition. Red indicates increased abundance of phosphosites, and green indicates decreased abundance of phosphosites. Graphics generated in Perseus (v. 1.6.14.0) (A) and RStudio (v. 4.2.0) using the Tidyverse package (1.3.1) (B) and IPA (09-2022 release) and enhanced in Adobe Illustrator (2022).

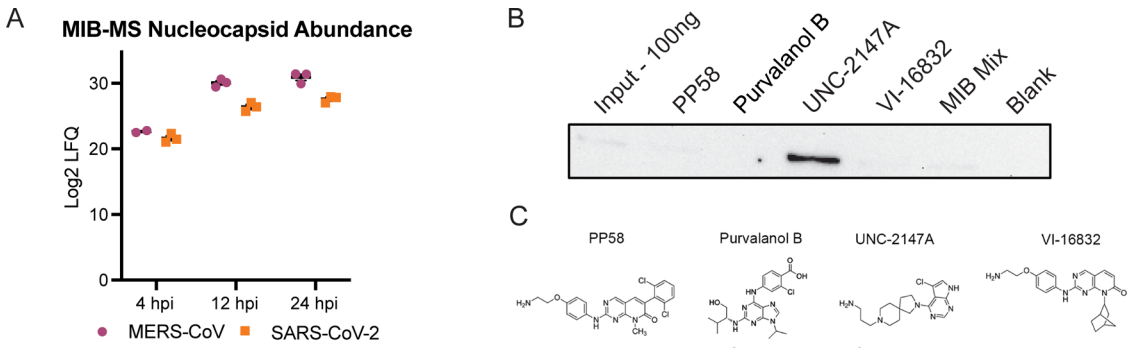

Figure 4. Nucleocapsid specifically binds to individual inhibitor beads. Purified SARS-CoV-2 nucleocapsid protein was incubated with individual inhibitor beads, blank beads, and MIB mix for 2 h prior to washing in a similar manner used for MIB-MS. Protein was eluted from beads, and binding was visualized via SDS-PAGE and Western blotting. (A) Quantification of nucleocapsid abundance identified during MIB-MS of MERS-CoV in purple and SARS-CoV-2 in orange. (B) Western blot of captured SARS-CoV-2 nucleocapsid protein following incubation with individual and mix of inhibitor beads that were used in MIB-MS. Input and blank beads included as positive and negative control. (C) Chemical structure of inhibitors used for MIB kinase capture and nucleocapsid pulldowns.[1] Average and standard error of the mean calculated and graphed in Prism 9 (A).

levels throughout the time course, while cluster II consisted of phosphosites that had increased phosphorylation levels (Figure 3a). Given that phosphorylation of specific residues can result in either increase or decrease in enzymatic activity, we performed a pathway analysis to identify how changes in phosphosite abundance may affect protein and signaling pathway activity. Upon analysis of the two clusters, we identified a number of activated pathways at 24 hpi that have been described in COVID-19 patients with severe disease, such as IL-6, IL-8, thrombin, PDGF, VEGF, and pulmonary fibrosis signaling (Figure 3b).[59] We additionally found that multiple kinase pathways were activated: MAPK, mTOR, PI3K/AKT, ERBB, and Ephrin receptor signaling. MAPK activation was further supported by increases in key phosphorylation sites of activation loop residues of both MAPK1 (pT185/pY187) and MAPK3 (pT202/pY204) at 12 and 24 hpi, with no statistically significant difference from mock at 4 hpi (Supplemental Data 3). mTOR signaling was of special interest given the increased binding of mTOR at 12 hpi in the MERS-CoV MIB-MS dataset, indicating a potential shared activated pathway between the two betacoronaviruses. Pathway analysis predicted activation of mTOR complex 1 (mTORC1) and mTORC2 at late timepoints in SARS-CoV-2 infection (Figure 3c), supported by changes in phosphosite abundance on EIF3A, EIF4B, EIF4E, RAP1B, RPS6, and RPTOR (Supplemental Data 5). This prediction was supported by increases in kinases associated with mTOR activation (PI3K/AKT) or decreases in those that oppose it (protein kinase A) (Figure 3b).

Comparison of SARS-CoV-2 MIBS-MS and Phosphoproteomics Datasets

Our MIB-MS kinome data indicated an overall decrease in kinase abundance after 24 hpi; however, by contrast, over 2000 phosphosites were up-regulated at 24 hpi and pathway analysis revealed an activation of many kinase pathways compared to mock infection (Figures 1–3). MAPK families showed an overall similar trend between the MIB-MS and phosphoproteomics datasets, with activity low in both at 4 hpi, but increased at later timepoints. Both MAPK1 and MAPK3 displayed increased MIB binding at 24 hpi, and pathway analysis based on the phosphoproteomics data predicted ERK/MAPK activation, further supported by increased activation loop phosphosite abundance. The largest difference between the MIB-MS and phosphoproteomics datasets was Ephrin receptor signaling, wherein a decrease in EPHA and EPHB binding to MIBs was observed, but pathway analysis predicted activation of Ephrin receptor signaling based on the phosphoproteomics dataset. ERBB signaling was also predicted to be activated in the pathway analysis; however, no significant kinome changes in the MIB-MS dataset were observed.

To further investigate potential factors that may have contributed to discordance between SARS-CoV-2 kinome and phosphoproteomic datasets, we searched for viral proteins identified in the MIB-MS datasets and found that the nucleocapsid protein (N) was the only viral protein consistently bound to MIB columns following both CoV infections across timepoints (Figure 4a, Supplemental Data 1 and 2). The CoV nucleocapsid protein can be phosphorylated on multiple residues, and recent work demonstrated that the SARS-CoV-2 nucleocapsid is capable of binding ATP.[60−62] Therefore, the nucleocapsid protein may have bound to the MIB-immobilized type I kinase inhibitors because these kinase inhibitors are ATP competitors. We identified multiple phosphosites on the SARS-CoV-2 nucleocapsid during the phosphoproteomics analysis; however, none of the phosphosites cluster around the proposed ATP-interacting residues (Figure S4). To validate the high amounts of nucleocapsid detected in our MIB-MS datasets, we incubated purified SARS-CoV-2 nucleocapsid with blank beads, the MIB resin, and individual kinase inhibitor beads. After washing and eluting specific proteins bound to these beads, we found that the nucleocapsid bound to the MIB mix but showed preferential binding to the UNC-2147A and weak binding to the VI-16832 and PP58 inhibitors, both type I kinase inhibitors (Figure 4b,c, Figure S5). This is the first instance of viral proteins binding to MIB, indicating a potential explanation for differences seen between MIB-MS and phosphoproteomic analyses.

Kinase Inhibitors Modulate CoV Replication

To study the potential effects of kinase inhibitors on CoV replication, we first performed an unbiased screen of both MERS-CoV and SARS-CoV-2 nanoluciferase (nLuc) expressing mutants against a panel of 187 compounds (5 μM) from the KCGS.[49] We additionally screened potential inhibitors of MERS-CoV replication at a 5 μM dose using a targeted ID3 set against host kinases that were identified as having changes in activity from the MERS-CoV MIB-MS dataset. Upon

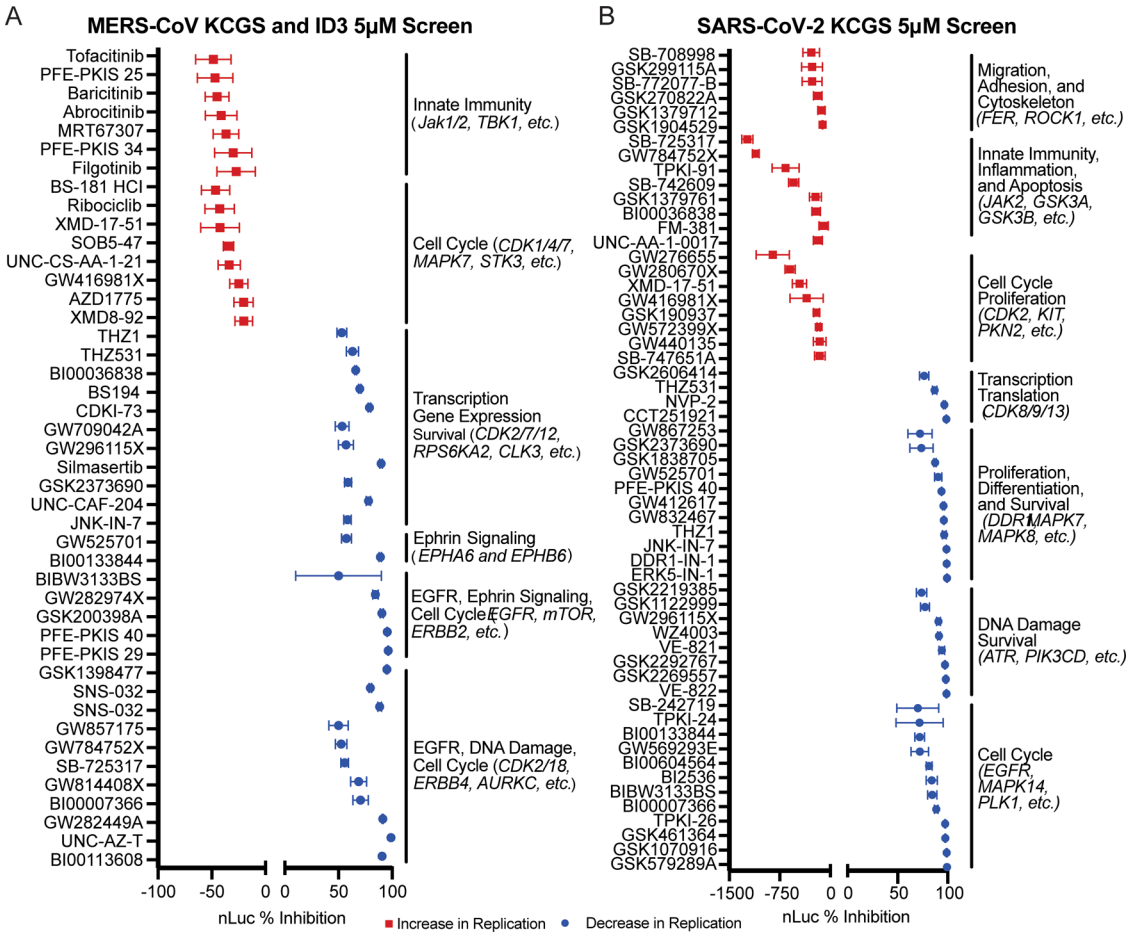

Figure 5. Kinase inhibitors alter CoV replication. Lung epithelial cells were treated with kinase inhibitors at a concentration of 5 μM 1 h prior to infection with MERS-CoV or SARS-CoV-2 nLuc-expressing viruses, respectively. Nanoluciferase readings were taken 48 hpi and normalized to DMSO treatment to calculate percent inhibition. Kinase inhibitors that exhibited an effect upon MERS-CoV nLuc replication in Calu3 cells (left). Kinase inhibitors that exhibited an effect upon SARS-CoV-2 nLuc replication in hACE2-A549 cells (right). Inhibitors that increased viral replication are in red while those that decreased viral replication are in blue. Representative target pathways highlighted on the right with kinase targets in italics. Average and standard error of the mean were calculated and graphed in Prism 9 (left and right).

completion of the screens for both CoVs, there was clear evidence of both viral growth inhibition and enhancement by several kinase inhibitors (Figure S6). Selection of kinase inhibitors with nLuc percent inhibition either >50% in MERS-CoV or >70% in SARS-CoV-2 highlighted transcription and EGFR and mTOR signaling, and the cell cycle as targetable pathways to reduce viral replication (Supplemental Data 6). In both CoVs, inhibition of kinases involved in innate immunity and some kinases affecting the cell cycle were found to increase replication (Figure 5). Untargeted KCGS screening was conducted to identify additional kinases whose activity was not predicted to change through kinome or phosphoproteomic analyses but may still contribute toward viral replication. These initial screens provided preliminary data to identify as many kinase targets as possible for further clinically advanced inhibitor screening.

While the KCGS and ID3 screens were insightful, the compounds in these libraries have limited clinical implications. Results from the kinome, phosphoproteomics, and chemogenomic datasets were used to assemble a CKS biased toward molecules that had advanced to clinical trials or had been approved as drugs by the FDA. This library of 93 compounds was screened at a 5 μM dose against MERS-CoV and SARS-CoV-2, resulting in 64 compounds that had greater than 70% or less than −50% inhibition of viral nLuc signal. The CKS identified ErbB kinases, CSNK2, and PI3K/mTOR as common inhibition targets for antiviral activity, while JAK and Syk inhibitors enhanced viral nLuc signal (Figure 6, Supplemental Data 7). MAPK inhibitors had mixed effects on CoV replication; however, most MAPK inhibitors decreased SARS-CoV-2 replication, mirroring activation seen in the MIB-MS and phosphoproteomic pathway analysis, indicating that the pathway may not be proviral and activation may be a secondary result of cell response to viral replication in MERS-CoV.

PI3K/mTOR Inhibitors Exhibit Potential for Broad-Acting CoV Antivirals

To validate inhibition and determine IC_{50} values, we performed dose−response curves on the kinase inhibitors of interest from the CKS. We included remdesivir, a nucleoside analog, as a positive control to compare antiviral activity of a direct-acting antiviral as compared to a kinase inhibitor.[23,63,64] Upon examination of dose−response curves, we found that the PI3K and mTOR inhibitors sapanisertib, samotolisib, and gedatolisib exhibited potent antiviral activity (nM range) in both CoVs, similar to the activity of remdesivir with minimal cytotoxicity (Table 1, Figure 7). Apitolisib and bimiralisib also

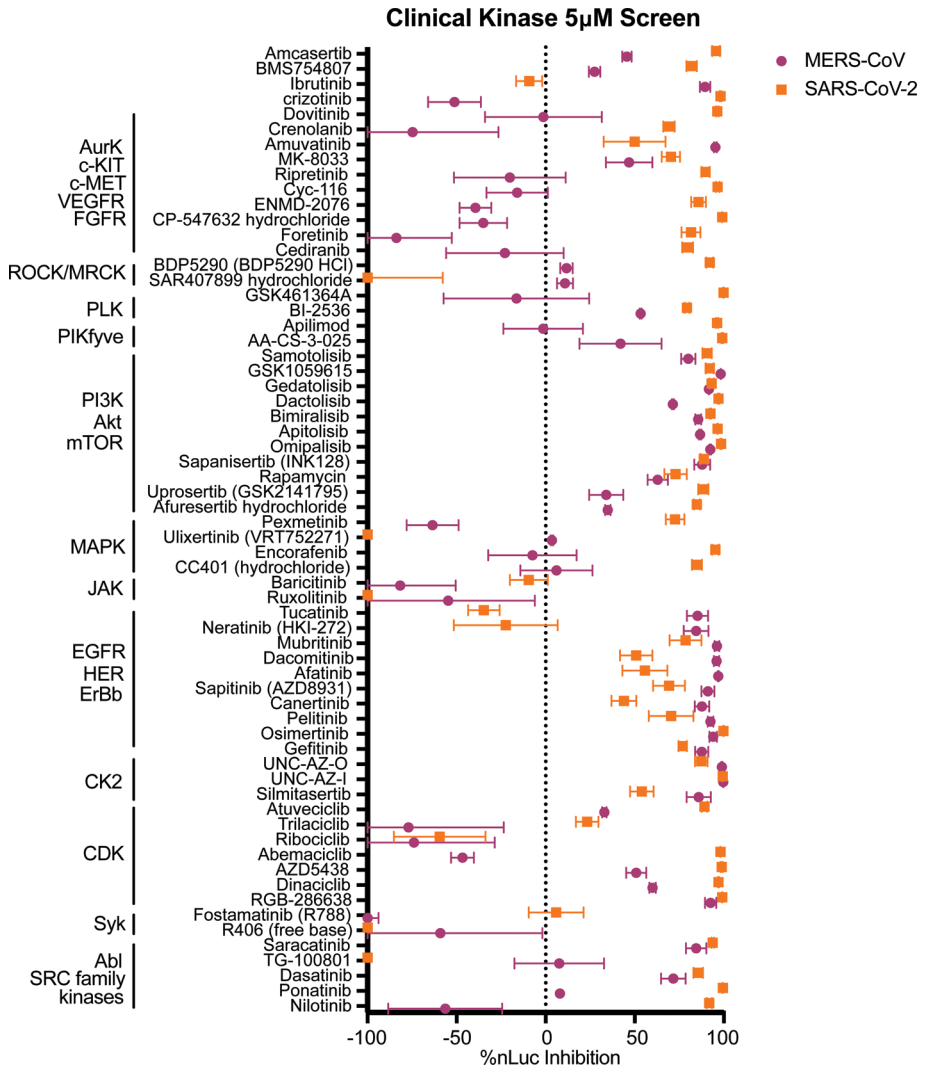

Figure 6. Clinically relevant kinase inhibitors are capable of inhibiting viral replication. A library of kinase inhibitors that are FDA approved or in clinical trials was selected based upon KCGS and MIB-MS datasets. Inhibitors were diluted to 5 μM, and cells were treated 1 h prior to infection with MERS-CoV or SARS-CoV-2 nLuc. Luciferase readings were performed at 48 hpi, and percent inhibition was calculated by comparing to uninfected cells. Inhibition or enhancement of MERS-CoV and SARS-CoV-2 replication following treatment with kinase inhibitors. MERS-CoV is represented in purple, and SARS-CoV-2 is represented in orange. Inhibitors are grouped by kinase target on the left. Average and standard error of the mean calculated and graphed in Prism 9.

demonstrated antiviral activity in both CoVs but not in the lower nM range as observed with the top three candidates. Omipalisib demonstrated cytotoxic activity in both cellular systems, ruling out its viability for repurposing. Dactolisib was only effective against SARS-CoV-2 nLuc signal, while GSK1059615 only reduced MERS-CoV nLuc signal in the nM ranges (Table 1).

MERS-CoV and SARS-CoV-2 Have Distinct Targetable Pathways for Drug Repurposing

While we were most interested in identifying broad-acting antivirals against MERS-CoV and SARS-CoV-2, there was also an interest in identifying virus-specific kinase inhibitors that reduced CoV replication. The EGFR and ErbB inhibitors that were included in our CKS panel exhibited antiviral activity against MERS-CoV in the low nM ranges; however, some demonstrated cytotoxic effects at similar concentrations. Canertinib, dacomitinib, and tucatinib all had IC_{50} values ranging from 25 to 166 nM with little or no toxicity, indicating possible repurposing for lineage 2C CoVs (Table 1, Figure S7). Of note, Calu3 cells have overactive ErbB2 signaling that contributes to their proliferation, so validation of antiviral effects of EGFR/ErbB inhibitors should be completed in another cell line or primary cells.[65] As previously demonstrated, PIKfyve kinase inhibitors exhibit antiviral activity in the low nM range for SARS-CoV-2 with minimal toxicity (Table 1).[25] However, the PIKfyve inhibitors tested here showed little efficacy against MERS-CoV replication (Figure S8).

We additionally found that CSNK2 inhibitors inhibited MERS-CoV at nM concentrations and SARS-CoV-2 at μM concentrations, as described previously (Figure S9).[28] Abl/Src family kinase inhibitors exhibited an antiviral effect upon SARS-CoV-2 at nM concentrations; however, these inhibitors are broad acting, so it is uncertain which of the target kinases may be essential for replication (Figure S9, Table 1). One of the CDK inhibitors, RGB-286638, demonstrated ~7-fold less antiviral activity against MERS-CoV compared to SARS-CoV-2; however, CDK inhibitors for SARS-CoV-2 were cytotoxic in

Table 1. Calculated Inhibitory and Cytotoxicity Concentrations of Top Performing Kinase Inhibitors[a]

identification		inhibition (nM)		cytotoxicity	
drug	target	IC50 MERS	IC50 SARS2	CC50 Calu3	CC50 A549
ponatinib	Abl		2635		~10 μM
dasatinib	Abl/Src	1310	191	>10 μM	>10 μM
saracatinib	Abl/Src	2183	292	6.8 μM	>10 μM
uprosertib	Akt	577		>10 μM	
ibrutinib	BTK	63		6.4 μM	
dinaciclib	CDK		20		4.1 μM
RGB-286638	CDK	643	90	>10 μM	12 nm
silmitasertib	CSNK2	530		>10 μM	
UNC-AZ-I	CSNK2	0.673	8	>10 μM	3 nM
UNC-AZ-O	CSNK2	188		>10 μM	
gefitinib	EGFR	396		~10 μM	
osimertinib	EGFR	110	851	~10 μM	>10 μM
sapitinib	EGFR/ErbB	82		~10 μM	
canertinib	EGFR/ErbB	114		>10 μM	
dacomitinib	EGFR/ErbB	25		>10 μM	
pelitinib	EGFR/ErbB	33		>10 μM	
afatinib	EGFR/ErbB	12		~10 μM	
mubritinib	HER2	7		>10 μM	
neratinib	HER2	12		~10 μM	
tucatinib	HER2	166		>10 μM	
omipalisib	PI3K	0.9	15	2.9 μM	434 nm
apitolisib	PI3K/mTOR	235	203	>10 μM	>10 μM
bimiralisib	PI3K/mTOR	182	628	>10 μm	>10 μM
dactolisib	PI3K/mTOR		12		5.5 μM
gedatolisib	PI3K/mTOR	30	10	>10 μm	>10 μM
GSK1059615	PI3K/mTOR	67		>10 μm	
samotolisib	PI3K/mTOR	30	22	>10 μm	6.1 μM
sapanisertib	mTORC1/2	9	7	>10 μM	>10 μM
AA-CS-3-025	PIKfyve		3.9		>10 μM
apilimod	PIKfyve		2.2		>10 μM
BI-2536	PLK		21.7		7.2 nM
GSK461364A	PLK		69.2		12.2 nM
CP-547632	VEGFR/FGFR		153		>10 μM
remdesivir	CoV RdRp	31	103	>10 μM	>10 μM

[a]IC_{50} values calculated following dosing of MERS-CoV- or SARS-CoV-2-infected cells with kinase inhibitors. CC_{50} values calculated following dosing of Calu3 and A549-hACE2 cells with kinase inhibitors. Cytotoxicity values that were outside the standard curve are noted as >10 μM, while those approaching CC50 at 10 μM are noted as ~10 μM. Blank cells indicate values not calculated due to poor viral growth inhibition.

A549-hACE2 cells. Cytotoxicity plagued PLK inhibitors as well for the SARS-CoV-2 assays, with minimal effect on MERS-CoV replication. Akt inhibitors were also of interest given that the inhibitor that SARS-CoV-2 N bound exhibits broad AGC family kinase capture (Figure 4); however, uprosertib only exhibited antiviral action against MERS-CoV at the mid-nM range (Figure S9, Supplemental Data 8 and 9).[1] MAPK inhibitors did not exhibit antiviral activity against either CoV in the nM range, like that of MERS-CoV KCGS results, indicating that increased MAPK activity seen in SARS-CoV-2 may be a result of the cellular response to CoV replication and infection rather than proviral (Supplemental Data 8 and 9).

DISCUSSION

Emerging CoVs, like SARS-CoV-2, and MERS-CoV, cause acute and chronic severe end stage lung disease outcomes after infection, necessitating the need for novel host-based therapies to reverse these outcomes. Host kinases represent important therapeutic targets for acute and potentially chronic viral infection of the lung, and several kinase inhibitors are used in COVID-19 patient care or are under evaluation.[66−68] A distinguishing feature of this study is the first employment of MIB-MS technology to capture kinases to measure host kinome response upon MERS-CoV and SARS-CoV-2 infection. Phosphoproteomic analysis over a SARS-CoV-2 time course was also employed to infer kinase activity for phosphorylation data. This analysis relies upon known kinase−substrate interactions and is, therefore, biased toward kinases that have well-characterized substrates. An advantage of the MIB-MS approach allows for direct measurement of changes in kinase abundance and/or activity following CoV infection. Surprisingly, our MIB-MS data recorded high amounts of nucleocapsid bound to MIB columns, potentially preventing some host kinases from being fully captured, due to competitive interactions of MIB with the viral nucleocapsid protein. Consequently, we most likely have underestimated kinase levels in our MIB-MS due to potential competition of MIB binding with viral N protein, which may have led to the lack of significant differences or exaggerated decreases in abundance especially at the 24 h timepoint compared to the mock controls. Although speculative, this hypothesis potentially explains the differences between inferred kinase activity levels from the phosphoproteomic data analysis and some of the kinases with decreased binding to MIB that were not less abundant in the proteomic dataset. Of those kinases that did have increased binding to MIB, there is clear evidence of activation of the mTOR and MAPK pathways following MERS-CoV and SARS-CoV-2 infection, respectively. Evidence of these changes in kinase activity following SARS-CoV-2 was further bolstered by phosphoproteomics analysis of infected A549-hACE2 cells, where there was increased phosphorylation of MAPK activation sites by 24 hpi.

While the goal of the MIB-MS analysis was to identify kinases, we found that CoV N proteins demonstrated reproducible binding to MIB in both datasets (Supplemental Data 1 and 2), with Log2 LFQ abundance increasing throughout the time course of infection (Figure 2). These findings were validated with pulldown experiments using purified recombinant N protein and individual inhibitor beads, finding specific binding to the UNC-2147A inhibitor. The nucleocapsid protein plays critical roles in virion nucleocapsid assembly and the production of progeny virions but also interacts with the viral replicase machinery to promote viral subgenomic and full-length RNA transcription.[69−72] Binding of CoV N to the MIB columns is potentially of high interest given recent studies that have highlighted ATP binding capabilities of N. The *N*-terminal domain (NTD) of N is involved in RNA binding, while the C-terminal domain (CTD) is thought to participate in resolving a secondary structure that has been shown to bind to ATP.[61,62] Furthermore, it is hypothesized that exposure of SARS-CoV-2 N to cytoplasmic concentrations of ATP may induce uncoating of the genomic RNA upon initial infection of the cell.[61] Given the hypothesized role of N

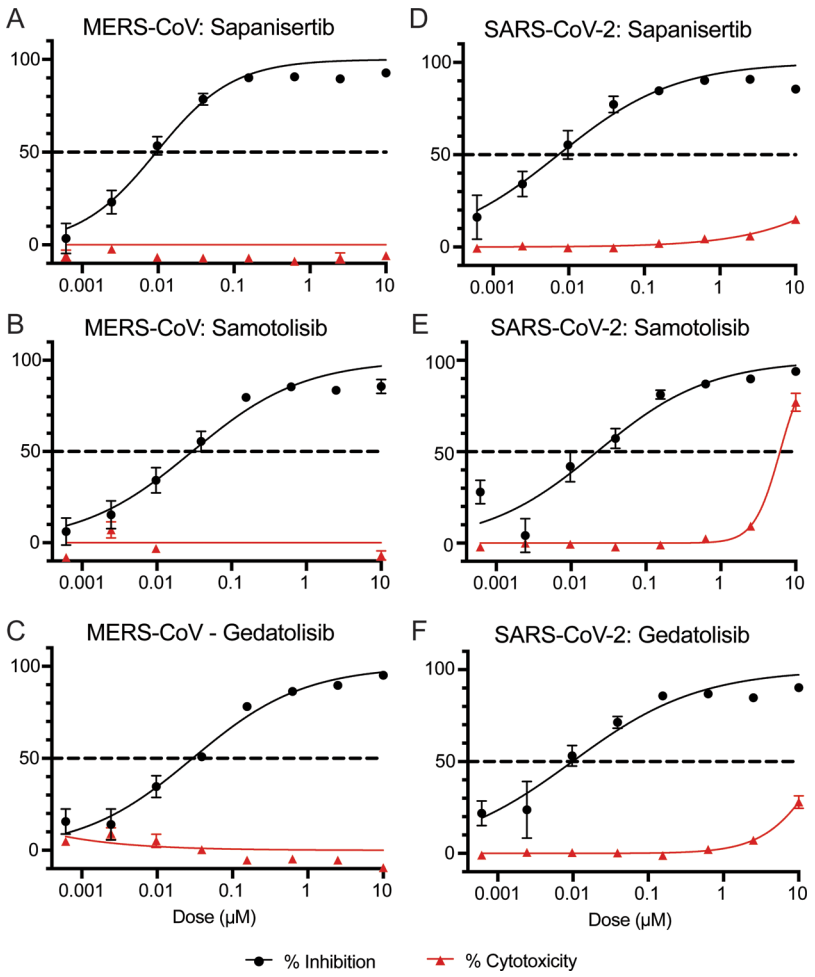

Figure 7. PI3K and mTOR inhibitors inhibit both MERS-CoV and SARS-CoV-2 replication at nM concentrations. Dose−response curves were performed by treating Calu3 and A549-hACE2 cells with serial dilutions of PI3K/mTOR kinase inhibitors 1 h prior to infection nLuc bearing MERS-CoV (A−C) or SARS-CoV-2 (D−F), respectively. Cells were incubated for 48 h prior to reading for nLuc and cytotoxicity measurements. Black closed circles and lines represent inhibition of viral nLuc expression, and red closed triangles and lines represent cytotoxicity measured by dead cell protease. Error bars represent the standard error of the mean. Average, standard error of the mean, and non-linear curve fits calculated and graphed in Prism 9.

as a potential chaperone protein in discontinuous transcription and its known role as a structural protein, it is an ideal candidate to target with small molecules or vaccines to disrupt multiple aspects of CoV replication.[73] The specific binding of viral proteins to MIBs has not been described previously and poses an interesting line of experiments in which MIB-MS may be used in a screen to identify potential small-molecule inhibitors of viral proteins. These findings provide a strategy to investigate the binding of nucleocapsid proteins from betacoronaviruses to preexisting kinase inhibitors and small-molecule libraries for further screening of direct-acting antiviral candidates. Expression of nucleocapsid isoforms with individual domains deleted will strengthen these studies to determine where small molecules are binding and allow for targeted molecule design to optimize potential nucleocapsid activity disruption.

Previous phosphoproteomic datasets have been generated from SARS-CoV-2-infected cell lines, induced alveolar type 2 (iAT2) cells, and animal models.[25−27,58,74−76] A phosphoproteomic analysis of nasopharyngeal swabs taken from uninfected and infected individuals with COVID-19 symptoms has also been performed.[77] Upon analysis of phosphoproteomic data, we identified similar activation of MAPK, PI3K/mTOR, and EGFR pathways to those described in Caco-2, Vero, and A549-hACE2 cells infected with SARS-CoV-2,[25,26,58] supporting pathway alterations across different immortalized tissue types and species. However, discrepancies in kinase activities were observed between A549-hACE2 and iAT2 phosphoproteomic datasets. Of note, the weak activation of mTOR described in iAT2 cells is similar to our inferred kinase activity data supporting both inhibition and activation of mTOR pathways.[27] A proteo-transcriptomics study of SARS-CoV-2-infected Huh7 cells also highlighted dysregulation in AKT/mTOR/HIF-1 signaling, further providing evidence outside of phosphoproteomic focused studies.[78] In animal models, there is further evidence supporting dysregulation of MAPK and CDK signaling following SARS-CoV-2 infection; however, the changes in kinase activity are temporal, indicating that specific stages in pathogenesis may be affecting kinase activities.[74,75] One study completed in MERS-CoV-infected Huh7 cells highlighted MAPK and PI3K/mTOR signaling as potential targetable pathways to reduce viral replication; however, we only identified increased mTOR binding at 12 hpi in our MIB-MS analysis.[79] More detailed kinase and phosphoproteomic comparisons should be examined between various primary cell tissue types and immortalized cells, especially as immortalized

cells display reprogrammed kinase signaling pathways and phosphoproteomic signatures.[80,81] Overall, our phosphoproteomic data, along with the previous studies, shows dysregulation of growth factor receptor signaling and survival pathways following SARS-CoV-2 infection across multiple cell types. This is unsurprising since the MAPK and mTOR pathways play essential roles in determining cell survival after viral infection.

Drug repurposing to reduce SARS-CoV-2 replication has been widely explored since the beginning of the pandemic, and kinase inhibitors such as imatinib, berzosertib, sorafenib, and vandetanib have been reported to inhibit CoV replication.[24−27,82,83] However, since kinases play essential roles in regulating cell cycle and growth, inhibitors must have a good selectivity index for antiviral effect on viral growth to minimize chances of off-target side effects. Due to this, we applied stringent cutoffs for proposing kinase inhibitors for repurposing, including compounds whose IC_{50} values were in nM ranges that phenocopied remdesivir and CC_{50} values that exceed the highest dose of kinase inhibitor screened, 10 μM. We tested multiple kinase inhibitors including some highlighted in previous studies, like dinaciclib, silmitasertib, and sorafenib. In many cases, however, these earlier studies either demonstrated CC_{50} values similar to IC_{50} values or were not effective in nM ranges similar to remdesivir.[25] Upon chemogenomic profiling of kinase inhibitors effects on CoV replication, we found that PI3K/mTOR inhibitors significantly reduced both MERS-CoV and SARS-CoV-2 replication at nM concentrations (Figure 7, Table 1). This has also been noted in Caco-2, Vero,[84] and A549 systems, but the activity of mTOR inhibitor VE-822 in iAT2 cells was not as effective,[27] perhaps reflecting host response differences or altered target specificity of VE-822, since not all PIK3/mTOR inhibitors we screened shared broad betacoronavirus antiviral activity (Figure 7, Table 1, Supplemental Data 8 and 9). While not broad acting, inhibitors of EGFR/ErbB kinases demonstrated efficacy in reducing MERS-CoV replication and PIKfyve inhibitors reduced SARS-CoV-2 replication, both in similar ranges to PI3K/mTOR inhibitors (Figure S7 and S8, Table 1). PIKfyve inhibitors have been previously described as potent SARS-CoV-2 replication inhibitors in vitro but actually exacerbated SARS-CoV-2 mortality in mice.[85] EGFR inhibitors have not been rigorously studied in the context of MERS-CoV. It should also be noted that differences in kinase inhibitor effects upon viral replication may be attributed to host kinase activity differences between the cell lines used for MERS-CoV and SARS-CoV-2 infections. We were unfortunately unable to reproduce SARS-CoV-2 infection in Calu3 cells similar to that of MERS-CoV to develop a robust replication system for kinase inhibitor screening; however, the titers achieved by SARS-CoV-2 infection of A549-hACE2 were similar to those of MERS-CoV in Calu3 cells. Future studies focused on PI3K/mTOR and EGFR inhibitors should focus on the mechanism of action and on characterizing their antiviral effects in more relevant *in vivo* and *ex vivo* infection models, like primary epithelial cells from the conducting airway and gas exchange regions of the lung.[86]

Our data mirrors similar growth inhibition at μM concentrations of JNK/MAPK inhibitors on either SARS-CoV-2 or MERS-CoV infection but indicates that PI3K/mTOR inhibition is more effective at lower compound concentrations.[25,26] Studies with the group 1 porcine epidemic diarrhea coronavirus (PEDV) showed that inhibition of the PI3K/AKT/GSK3 or PI3K/AKT/mTOR pathway increased viral replication, indicating that the antiviral activities of PI3K/mTOR inhibitors may be betacoronavirus specific.[87,88] PI3K/AKT/mTOR signaling plays a central role in cell survival, so there may be an enhancement of apoptosis in infected cells, potentially reducing the virus's ability to maximize the production of new progeny. We found activation of mTOR complexes in our pathway analysis, which are involved in regulation of the cytoskeleton, autophagy, translation, and activation of pro-survival pathways, indicating that mTOR activation may be contributing to inhibition of apoptosis of SARS-CoV-2-infected cells.[89] Experiments in SARS-CoV have demonstrated that both the JNK and PI3K pathways were necessary in promoting cell survival *in vitro* to establish persistent infection of host cells without induction of apoptotic effect.[90] The importance of the PI3K pathway was further highlighted by a study in MERS-CoV in which inhibition of both the MAPK and PI3K pathways demonstrated an antiviral effect.[79] Additionally, PI3K signaling has been shown to regulate endocytosis, so there may be a reduction in viral uptake following treatment with PI3K/mTOR inhibitors.[91] The PI3K/AKT pathway may also be a viable target for reducing SARS-CoV-2-related coagulopathy, as inhibition of PI3K has been shown to suppress platelet activation, revealing a potential multifaceted role for PI3K/mTOR inhibitors as CoV therapeutics for pathogenesis as well.[92]

The largest caveat to this and other similar works is the use of continuous cell lines as screening models, and potential limited translation to *in vivo* models. Cell lines have homogenous populations that exhibit aberrant kinase activity and may not recapitulate certain infection dynamics that would be seen in diverse cell populations seen in primary lung tissues. Recent work evaluating the kinase response to SARS-CoV-2-infected mice, rhesus macaques, and humans has highlighted similar dysregulated pathways as those in our study.[74,76,77] However, it is unclear if signaling by shared pathways is coordinately regulated following infection since there are differing results depending on the model platform. For example, in the mouse and rhesus macaque lung model, there is upregulation of the PI3K/AKT/mTOR, p38, and MAPK signaling pathways; however, the AKT pathway is downregulated in nasopharyngeal swabs collected from SARS-CoV-2 patients.[74,76,77] One aspect of the dysregulation in these models is that it may be temporal and compartment specific; thus, it is difficult to compare to our cellular data due to the large cytopathic effect seen by 24 hpi *in vitro*. An ideal model for profiling of the host kinome response to CoV infection would allow ease of experimental use to test potential kinase inhibitors and multiple timepoints while recapitulating genetic and cell population diversity. For this reason, we believe future kinome and phosphoproteome studies should be conducted in human airway epithelial *ex vivo* cultures, which have been used to study CoV replication in the lung; however, there has been no study on the kinase response to infection.[28] Profiling of host kinase responses in a primary human airway epithelial model is also of interest given that they will exhibit less irregular kinase activity compared to immortal cell lines.

Our study focuses specifically on evaluating kinase inhibitor treatment effect upon viral replication; however, as seen with the emergency use authorization of JAK inhibitors, targeting of kinases may serve to alter the more complex pathogenesis programs associated with acute and chronic infection.[93,94] Many of the kinase cascades are known to interplay within

cytokine and innate immune signaling, and kinases play key roles in ARDS and pulmonary fibrosis, suggesting that targeted kinase inhibitors offer hope for treating late-stage disease outcomes after COVID-19 as well.[95−97] Evidence of reduction of SARS-CoV-2 pathogenesis by kinase inhibitors has been supported for fostamatinib, an inhibitor of SYK, for reducing platelet activation following SARS-CoV-2, and nintedanib, a VEGFR/FGFR/PDGFR inhibitor, which is commonly used to treat idiopathic pulmonary fibrosis.[14,98−100] In MERS-CoV infection, targeting of the unfolded protein response via inhibition of PERK was found to reduce viral replication in primary cells and acute pathogenesis in a murine model.[101] Future kinome studies in primary cells and murine models will provide the opportunity to evaluate the ability of kinase inhibitors to dampen cytokine storm and immunopathology. We are actively exploring these routes to truly understand the dependence of CoVs on host kinase activity and potential host-targeted, broad-acting therapies that can be leveraged in response to currently circulating and emergent CoVs.

■ ASSOCIATED CONTENT

Data Availability Statement

The proteomics, phosphoproteomics, and MIB-MS datasets generated in this study are available in the Proteomics Identification Database (PRIDE) repository under project identifiers PXD040897 (Proteome and Phosphoproteome) and PXD040901 (MIB-MS).

Supporting Information

The Supporting Information is available free of charge at https://pubs.acs.org/doi/10.1021/acs.jproteome.3c00182.

(Supplemental Figure 1) PCA of MERS-CoV and SARS-CoV-2 MIB-MS; (Supplemental Figure 2) heatmaps of MERS-CoV and SARS-CoV-2 MIB-MS data; (Supplemental Figure 3) PCA and volcano plots of SARS-CoV-2 phosphoproteomic data; (Supplemental Figure 4) identified SARS-CoV-2 nucleocapsid phosphosites; (Supplemental Figure 5) Western blot of eluted SARS-CoV-2 nucleocapsid from MIB pulldown; (Supplemental Figure 6) MERS-CoV KCGS and ID3 screen and SARS-CoV-2 KCGS screen); (Supplemental Figure 7) EGFR/ErbB dose−response curves; (Supplemental Figure 8) PIKfyve dose−response curves; (Supplemental Figure 9) additional dose−response curves (PDF)

MERS-CoV MIB-MS data (XLSX)

SARS-CoV-2 MIB-MS data (XLSX)

SARS-CoV-2 phosphoproteomics data (XLSX)

SARS-CoV-2 proteomics data (XLSX)

SARS-CoV-2 IPA (XLSX)

MERS-CoV KCGS and ID3 screen and SARS-CoV-2 KCGS screen (XLSX)

MERS-CoV and SARS-CoV-2 CKS drug screen (XLSX)

MERS-CoV dose−response curves (XLSX)

SARS-CoV-2 dose−response curves (XLSX)

■ AUTHOR INFORMATION

Corresponding Author

Ralph S. Baric − *Department of Microbiology and Immunology, School of Medicine, University of North Carolina at Chapel Hill, Chapel Hill, North Carolina 27599-7290, United States; Department of Epidemiology, Gillings School of Public Health, University of North Carolina at Chapel Hill, Chapel Hill, North Carolina 27599-7400, United States; Lineberger Comprehensive Cancer Center, University of North Carolina at Chapel Hill, Chapel Hill, North Carolina 27514, United States;* Email: rbaric@email.unc.edu

Authors

Ethan J. Fritch − *Department of Microbiology and Immunology, School of Medicine, University of North Carolina at Chapel Hill, Chapel Hill, North Carolina 27599-7290, United States;* orcid.org/0000-0003-1096-8958

Angie L. Mordant − *UNC Michael Hooker Proteomics Core, University of North Carolina at Chapel Hill, Chapel Hill, North Carolina 27599, United States*

Thomas S.K. Gilbert − *Department of Pharmacology, School of Medicine, University of North Carolina at Chapel Hill, Chapel Hill, North Carolina 27599-7365, United States;* orcid.org/0000-0002-6833-6788

Carrow I. Wells − *Structural Genomics Consortium, Department of Chemical Biology and Medicinal Chemistry, UNC Eshelman School of Pharmacy, University of North Carolina at Chapel Hill, Chapel Hill, North Carolina 27599-7264, United States*

Xuan Yang − *Structural Genomics Consortium, Department of Chemical Biology and Medicinal Chemistry, UNC Eshelman School of Pharmacy, University of North Carolina at Chapel Hill, Chapel Hill, North Carolina 27599-7264, United States*

Natalie K. Barker − *UNC Michael Hooker Proteomics Core, University of North Carolina at Chapel Hill, Chapel Hill, North Carolina 27599, United States*

Emily A. Madden − *Department of Microbiology and Immunology, School of Medicine, University of North Carolina at Chapel Hill, Chapel Hill, North Carolina 27599-7290, United States*

Kenneth H. Dinnon, III − *Department of Microbiology and Immunology, School of Medicine, University of North Carolina at Chapel Hill, Chapel Hill, North Carolina 27599-7290, United States*

Yixuan J. Hou − *Department of Epidemiology, Gillings School of Public Health, University of North Carolina at Chapel Hill, Chapel Hill, North Carolina 27599-7400, United States*

Longping V. Tse − *Department of Epidemiology, Gillings School of Public Health, University of North Carolina at Chapel Hill, Chapel Hill, North Carolina 27599-7400, United States*

Izabella N. Castillo − *Department of Microbiology and Immunology, School of Medicine, University of North Carolina at Chapel Hill, Chapel Hill, North Carolina 27599-7290, United States*

Amy C. Sims − *Department of Epidemiology, Gillings School of Public Health, University of North Carolina at Chapel Hill, Chapel Hill, North Carolina 27599-7400, United States*

Nathaniel J. Moorman − *Department of Microbiology and Immunology, School of Medicine, University of North Carolina at Chapel Hill, Chapel Hill, North Carolina 27599-7290, United States; Lineberger Comprehensive Cancer Center, University of North Carolina at Chapel Hill, Chapel Hill, North Carolina 27514, United States*

Premkumar Lakshmanane − *Department of Microbiology and Immunology, School of Medicine, University of North*

Carolina at Chapel Hill, Chapel Hill, North Carolina 27599-7290, United States

Timothy M. Willson − *Structural Genomics Consortium, Department of Chemical Biology and Medicinal Chemistry, UNC Eshelman School of Pharmacy, University of North Carolina at Chapel Hill, Chapel Hill, North Carolina 27599-7264, United States;* orcid.org/0000-0003-4181-8223

Laura E. Herring − *UNC Michael Hooker Proteomics Core, University of North Carolina at Chapel Hill, Chapel Hill, North Carolina 27599, United States; Department of Pharmacology, School of Medicine, University of North Carolina at Chapel Hill, Chapel Hill, North Carolina 27599-7365, United States;* orcid.org/0000-0003-4496-7312

Lee M. Graves − *UNC Michael Hooker Proteomics Core, University of North Carolina at Chapel Hill, Chapel Hill, North Carolina 27599, United States; Department of Pharmacology, School of Medicine, University of North Carolina at Chapel Hill, Chapel Hill, North Carolina 27599-7365, United States; Lineberger Comprehensive Cancer Center, University of North Carolina at Chapel Hill, Chapel Hill, North Carolina 27514, United States;* orcid.org/0000-0002-4736-9855

Complete contact information is available at: https://pubs.acs.org/10.1021/acs.jproteome.3c00182

Notes

The authors declare no competing financial interest.

■ ACKNOWLEDGMENTS

We would like to thank Zijie Zhang for assistance with compound plating and distribution. We would like to thank Dr. Brea Kaseanna-Lanae Hampton-Brown, Department of Genetics, University of North Carolina at Chapel Hill, for technical assistance with R programming. The research was supported by a READDI grant at the University of North Carolina at Chapel Hill appropriated by the North Carolina General Assembly. The work was also supported by NIH grant AI110700 and AI142759 to R.S.B., T32 AI007419 to E.J.F., and R01GM138520 and P30 CA016086 to L.M.G. Research reported in this publication was supported by the NIH Illuminating the Druggable Genome 1U24DK116204-01. The UNC Michael Hooker Proteomics Core is supported in part by NCI Center Core Support Grant (2P30CA016086-45) to the UNC Lineberger Comprehensive Cancer Center. The Structural Genomics Consortium is a registered charity (no. 1097737) that receives funds from Bayer AG, Boehringer Ingelheim, Bristol Myers Squibb, Genentech, Genome Canada through Ontario Genomics Institute [OGI-196], EU/EFPIA/OICR/McGill/KTH/Diamond Innovative Medicines Initiative 2 Joint Undertaking [EUbOPEN grant 875510], Janssen, Merck KGaA (aka EMD in Canada and US), Pfizer, and Takeda.

■ REFERENCES

(1) Collins, K. A. L.; Stuhlmiller, T. J.; Zawistowski, J. S.; East, M. P.; Pham, T. T.; Hall, C. R.; Goulet, D. R.; Bevill, S. M.; Angus, S. P.; Velarde, S. H.; Sciaky, N.; Oprea, T. I.; Graves, L. M.; Johnson, G. L.; Gomez, S. M. Proteomic analysis defines kinase taxonomies specific for subtypes of breast cancer. *Oncotarget* **2018**, *9*, 15480−15497.

(2) Metz, K. S.; Deoudes, E. M.; Berginski, M. E.; Jimenez-Ruiz, I.; Aksoy, B. A.; Hammerbacher, J.; Gomez, S. M.; Phanstiel, D. H. Coral: Clear and Customizable Visualization of Human Kinome Data. *Cell Syst.* **2018**, *7*, 347−350.e1.

(3) McIntosh, K.; Kapikian, A. Z.; Turner, H. C.; Hartley, J. W.; Parrott, R. H.; Chanock, R. M. Seroepidemiologic studies of coronavirus infection in adults and children. *Am. J. Epidemiol.* **1970**, *91*, 585−592.

(4) van der Hoek, L.; Pyrc, K.; Jebbink, M. F.; Vermeulen-Oost, W.; Berkhout, R. J. M.; Wolthers, K. C.; Wertheim-van Dillen, P. M. E.; Kaandorp, J.; Spaargaren, J.; Berkhout, B. Identification of a new human coronavirus. *Nat. Med.* **2004**, *10*, 368−373.

(5) Pijpers, A.; van Nieuwstadt, A. P.; Terpstra, C.; Verheijden, J. H. Porcine epidemic diarrhoea virus as a cause of persistent diarrhoea in a herd of breeding and finishing pigs. *Vet. Rec.* **1993**, *132*, 129−131.

(6) Ksiazek, T. G.; Erdman, D.; Goldsmith, C. S.; Zaki, S. R.; Peret, T.; Emery, S.; Tong, S.; Urbani, C.; Comer, J. A.; Lim, W.; Rollin, P. E.; Dowell, S. F.; Ling, A.-E.; Humphrey, C. D.; Shieh, W.-J.; Guarner, J.; Paddock, C. D.; Roca, P.; Fields, B.; DeRisi, J.; Yang, J. Y.; Cox, N.; Hughes, J. M.; LeDuc, J. W.; Bellini, W. J.; Anderson, L. J.; The SARS Working Group. A novel coronavirus associated with severe acute respiratory syndrome. *N. Engl. J. Med.* **2003**, *348*, 1953−1966.

(7) Zaki, A. M.; van Boheemen, S.; Bestebroer, T. M.; Osterhaus, A. D. M. E.; Fouchier, R. A. M. Isolation of a novel coronavirus from a man with pneumonia in Saudi Arabia. *N. Engl. J. Med.* **2012**, *367*, 1814−1820.

(8) Zhu, N.; Zhang, D.; Wang, W.; Li, X.; Yang, B.; Song, J.; Zhao, X.; Huang, B.; Shi, W.; Lu, R.; Niu, P.; Zhan, F.; Ma, X.; Wang, D.; Xu, W.; Wu, G.; Gao, G. F.; Tan, W.; China Novel Coronavirus Investigating Research Team. A Novel Coronavirus from Patients with Pneumonia in China, 2019. *N. Engl. J. Med.* **2020**, *382*, 727−733.

(9) WHO *MERS Situation Update*. http://applications.emro.who.int/docs/EMROPub-MERS-SEP-2019-EN.pdf?ua=1&ua=1 **2019** (accessed August 19, 2022).

(10) Perlman, S.; Zumla, A. MERS-CoV in Africa-an enigma with relevance to COVID-19. *Lancet Infect. Dis.* **2021**, *21*, 303−305.

(11) WHO *WHO Coronavirus (COVID-19) Dashboard* https://covid19.who.int/.

(12) Corbett, K. S.; Edwards, D. K.; Leist, S. R.; Abiona, O. M.; Boyoglu-Barnum, S.; Gillespie, R. A.; Himansu, S.; Schäfer, A.; Ziwawo, C. T.; DiPiazza, A. T.; Dinnon, K. H.; Elbashir, S. M.; Shaw, C. A.; Woods, A.; Fritch, E. J.; Martinez, D. R.; Bock, K. W.; Minai, M.; Nagata, B. M.; Hutchinson, G. B.; Wu, K.; Henry, C.; Bahl, K.; Garcia-Dominguez, D.; Ma, L.; Renzi, I.; Kong, W. P.; Schmidt, S. D.; Wang, L.; Zhang, Y.; Phung, E.; Chang, L. A.; Loomis, R. J.; Altaras, N. E.; Narayanan, E.; Metkar, M.; Presnyak, V.; Liu, C.; Louder, M. K.; Shi, W.; Leung, K.; Yang, E. S.; West, A.; Gully, K. L.; Stevens, L. J.; Wang, N.; Wrapp, D.; Doria-Rose, N. A.; Stewart-Jones, G.; Bennett, H.; Alvarado, G. S.; Nason, M. C.; Ruckwardt, T. J.; McLellan, J. S.; Denison, M. R.; Chappell, J. D.; Moore, I. N.; Morabito, K. M.; Mascola, J. R.; Baric, R. S.; Carfi, A.; Graham, B. S. SARS-CoV-2 mRNA vaccine design enabled by prototype pathogen preparedness. *Nature* **2020**, *586*, 567−571.

(13) Cao, Y.; Wang, J.; Jian, F.; Xiao, T.; Song, W.; Yisimayi, A.; Huang, W.; Li, Q.; Wang, P.; An, R.; Wang, J.; Wang, Y.; Niu, X.; Yang, S.; Liang, H.; Sun, H.; Li, T.; Yu, Y.; Cui, Q.; Liu, S.; Yang, X.; Du, S.; Zhang, Z.; Hao, X.; Shao, F.; Jin, R.; Wang, X.; Xiao, J.; Wang, Y.; Xie, X. S. Omicron escapes the majority of existing SARS-CoV-2 neutralizing antibodies. *Nature* **2022**, *602*, 657−663.

(14) Dinnon, K. H., III; Leist, S. R.; Okuda, K.; Dang, H.; Fritch, E. J.; Gully, K. L.; De la Cruz, G.; Evangelista, M. D.; Asakura, T.; Gilmore, R. C.; Hawkins, P.; Nakano, S.; West, A.; Schäfer, A.; Gralinski, L. E.; Everman, J. L.; Sajuthi, S. P.; Zweigart, M. R.; Dong, S.; McBride, J.; Cooley, M. R.; Hines, J. B.; Love, M. K.; Groshong, S. D.; VanSchoiack, A.; Phelan, S. J.; Liang, Y.; Hether, T.; Leon, M.; Zumwalt, R. E.; Barton, L. M.; Duval, E. J.; Mukhopadhyay, S.; Stroberg, E.; Borczuk, A.; Thorne, L. B.; Sakthivel, M. K.; Lee, Y. Z.; Hagood, J. S.; Mock, J. R.; Seibold, M. A.; O'Neal, W. K.; Montgomery, S. A.; Boucher, R. C.; Baric, R. S. SARS-CoV-2 infection produces chronic pulmonary epithelial and immune cell

dysfunction with fibrosis in mice. *Sci. Transl. Med.* **2022**, No. eabo5070.
(15) Nalbandian, A.; Sehgal, K.; Gupta, A.; Madhavan, M. V.; McGroder, C.; Stevens, J. S.; Cook, J. R.; Nordvig, A. S.; Shalev, D.; Sehrawat, T. S.; Ahluwalia, N.; Bikdeli, B.; Dietz, D.; Der-Nigoghossian, C.; Liyanage-Don, N.; Rosner, G. F.; Bernstein, E. J.; Mohan, S.; Beckley, A. A.; Seres, D. S.; Choueiri, T. K.; Uriel, N.; Ausiello, J. C.; Accili, D.; Freedberg, D. E.; Baldwin, M.; Schwartz, A.; Brodie, D.; Garcia, C. K.; Elkind, M. S. V.; Connors, J. M.; Bilezikian, J. P.; Landry, D. W.; Wan, E. Y. Post-acute COVID-19 syndrome. *Nat. Med.* **2021**, *27*, 601−615.
(16) Ge, X. Y.; Li, J. L.; Yang, X. L.; Chmura, A. A.; Zhu, G.; Epstein, J. H.; Mazet, J. K.; Hu, B.; Zhang, W.; Peng, C.; Zhang, Y. J.; Luo, C. M.; Tan, B.; Wang, N.; Zhu, Y.; Crameri, G.; Zhang, S. Y.; Wang, L. F.; Daszak, P.; Shi, Z. L. Isolation and characterization of a bat SARS-like coronavirus that uses the ACE2 receptor. *Nature* **2013**, *503*, 535−538.
(17) Menachery, V. D.; Yount, B. L., Jr.; Debbink, K.; Agnihothram, S.; Gralinski, L. E.; Plante, J. A.; Graham, R. L.; Scobey, T.; Ge, X. Y.; Donaldson, E. F.; Randell, S. H.; Lanzavecchia, A.; Marasco, W. A.; Shi, Z. L.; Baric, R. S. A SARS-like cluster of circulating bat coronaviruses shows potential for human emergence. *Nat. Med.* **2015**, *21*, 1508−1513.
(18) Menachery, V. D.; Yount, B. L., Jr.; Sims, A. C.; Debbink, K.; Agnihothram, S. S.; Gralinski, L. E.; Graham, R. L.; Scobey, T.; Plante, J. A.; Royal, S. R.; Swanstrom, J.; Sheahan, T. P.; Pickles, R. J.; Corti, D.; Randell, S. H.; Lanzavecchia, A.; Marasco, W. A.; Baric, R. S. SARS-like WIV1-CoV poised for human emergence. *Proc. Natl. Acad. Sci. U. S. A.* **2016**, *113*, 3048−3053.
(19) Temmam, S.; Vongphayloth, K.; Baquero, E.; Munier, S.; Bonomi, M.; Regnault, B.; Douangboubpha, B.; Karami, Y.; Chrétien, D.; Sanamxay, D.; Xayaphet, V.; Paphaphanh, P.; Lacoste, V.; Somlor, S.; Lakeomany, K.; Phommavanh, N.; Pérot, P.; Dehan, O.; Amara, F.; Donati, F.; Bigot, T.; Nilges, M.; Rey, F. A.; van der Werf, S.; Brey, P. T.; Eloit, M. Bat coronaviruses related to SARS-CoV-2 and infectious for human cells. *Nature* **2022**, *604*, 330−336.
(20) Yen, M.; Ren, J.; Liu, Q.; Glassman, C. R.; Sheahan, T. P.; Picton, L. K.; Moreira, F. R.; Rustagi, A.; Jude, K. M.; Zhao, X.; Blish, C. A.; Baric, R. S.; Su, L. L.; Garcia, K. C. Facile discovery of surrogate cytokine agonists. *Cell* **2022**, *185*, 1414−1430.e19.
(21) Schäfer, A.; Martinez, D. R.; Won, J. J.; Meganck, R. M.; Moreira, F. R.; Brown, A. J.; Gully, K. L.; Zweigart, M. R.; Conrad, W. S.; May, S. R.; Dong, S.; Kalla, R.; Chun, K.; Du Pont, V.; Babusis, D.; Tang, J.; Murakami, E.; Subramanian, R.; Barrett, K. T.; Bleier, B. J.; Bannister, R.; Feng, J. Y.; Bilello, J. P.; Cihlar, T.; Mackman, R. L.; Montgomery, S. A.; Baric, R. S.; Sheahan, T. P. Therapeutic treatment with an oral prodrug of the remdesivir parental nucleoside is protective against SARS-CoV-2 pathogenesis in mice. *Sci. Transl. Med.* **2022**, *14*, No. eabm3410.
(22) Sheahan, T. P.; Sims, A. C.; Zhou, S.; Graham, R. L.; Pruijssers, A. J.; Agostini, M. L.; Leist, S. R.; Schäfer, A.; Dinnon, K. H., III; Stevens, L. J.; Chappell, J. D.; Lu, X.; Hughes, T. M.; George, A. S.; Hill, C. S.; Montgomery, S. A.; Brown, A. J.; Bluemling, G. R.; Natchus, M. G.; Saindane, M.; Kolykhalov, A. A.; Painter, G.; Harcourt, J.; Tamin, A.; Thornburg, N. J.; Swanstrom, R.; Denison, M. R.; Baric, R. S. An orally bioavailable broad-spectrum antiviral inhibits SARS-CoV-2 in human airway epithelial cell cultures and multiple coronaviruses in mice. *Sci. Transl. Med.* **2020**, *12*, No. eabb5883.
(23) Pruijssers, A. J.; George, A. S.; Schäfer, A.; Leist, S. R.; Gralinksi, L. E.; Dinnon, K. H., III; Yount, B. L.; Agostini, M. L.; Stevens, L. J.; Chappell, J. D.; Lu, X.; Hughes, T. M.; Gully, K.; Martinez, D. R.; Brown, A. J.; Graham, R. L.; Perry, J. K.; Du Pont, V.; Pitts, J.; Ma, B.; Babusis, D.; Murakami, E.; Feng, J. Y.; Bilello, J. P.; Porter, D. P.; Cihlar, T.; Baric, R. S.; Denison, M. R.; Sheahan, T. P. Remdesivir Inhibits SARS-CoV-2 in Human Lung Cells and Chimeric SARS-CoV Expressing the SARS-CoV-2 RNA Polymerase in Mice. *Cell Rep.* **2020**, *32*, No. 107940.
(24) Weston, S.; Coleman, C. M.; Haupt, R.; Logue, J.; Matthews, K.; Li, Y.; Reyes, H. M.; Weiss, S. R.; Frieman, M. B. Broad Anti-coronavirus Activity of Food and Drug Administration-Approved Drugs against SARS-CoV-2 In Vitro and SARS-CoV In Vivo. *J. Virol.* **2020**, *94*, 10−1128.
(25) Bouhaddou, M.; Memon, D.; Meyer, B.; White, K. M.; Rezelj, V. V.; Marrero, C. M.; Polacco, B. J.; Melnyk, J. E.; Ulferts, S.; Kaake, R. M.; Batra, J.; Richards, A. L.; Stevenson, E.; Gordon, D. E.; Rojc, A.; Obernier, K.; Fabius, J. M.; Soucheray, M.; Miorin, L.; Moreno, E.; Koh, C.; Tran, Q. D.; Hardy, A.; Robinot, R.; Vallet, T.; Nilsson-Payant, B. E.; Hernandez-Armenta, C.; Dunham, A.; Weigang, S.; Knerr, J.; Modak, M.; Quintero, D.; Zhou, Y.; Dugourd, A.; Valdeolivas, A.; Patil, T.; Li, Q.; Hüttenhain, R.; Cakir, M.; Muralidharan, M.; Kim, M.; Jang, G.; Tutuncuoglu, B.; Hiatt, J.; Guo, J. Z.; Xu, J.; Bouhaddou, S.; Mathy, C. J. P.; Gaulton, A.; Manners, E. J.; Félix, E.; Shi, Y.; Goff, M.; Lim, J. K.; McBride, T.; O'Neal, M. C.; Cai, Y.; Chang, J. C. J.; Broadhurst, D. J.; Klippsten, S.; De Wit, E.; Leach, A. R.; Kortemme, T.; Shoichet, B.; Ott, M.; Saez-Rodriguez, J.; tenOever, B. R.; Mullins, R. D.; Fischer, E. R.; Kochs, G.; Grosse, R.; García-Sastre, A.; Vignuzzi, M.; Johnson, J. R.; Shokat, K. M.; Swaney, D. L.; Beltrao, P.; Krogan, N. J. The Global Phosphorylation Landscape of SARS-CoV-2 Infection. *Cell* **2020**, *182*, 685−712.e19.
(26) Klann, K.; Bojkova, D.; Tascher, G.; Ciesek, S.; Münch, C.; Cinatl, J. Growth Factor Receptor Signaling Inhibition Prevents SARS-CoV-2 Replication. *Mol. Cell* **2020**, *80*, 164−174.e4.
(27) Hekman, R. M.; Hume, A. J.; Goel, R. K.; Abo, K. M.; Huang, J.; Blum, B. C.; Werder, R. B.; Suder, E. L.; Paul, I.; Phanse, S.; Youssef, A.; Alysandratos, K. D.; Padhorny, D.; Ojha, S.; Mora-Martin, A.; Kretov, D.; Ash, P. E. A.; Verma, M.; Zhao, J.; Patten, J. J.; Villacorta-Martin, C.; Bolzan, D.; Perea-Resa, C.; Bullitt, E.; Hinds, A.; Tilston-Lunel, A.; Varelas, X.; Farhangmehr, S.; Braunschweig, U.; Kwan, J. H.; McComb, M.; Basu, A.; Saeed, M.; Perissi, V.; Burks, E. J.; Layne, M. D.; Connor, J. H.; Davey, R.; Cheng, J.-X.; Wolozin, B. L.; Blencowe, B. J.; Wuchty, S.; Lyons, S. M.; Kozakov, D.; Cifuentes, D.; Blower, M.; Kotton, D. N.; Wilson, A. A.; Mühlberger, E.; Emili, A. Actionable Cytopathogenic Host Responses of Human Alveolar Type 2 Cells to SARS-CoV-2. *Mol. Cell* **2020**, *80*, 1104−1122.e9.
(28) Yang, X.; Dickmander, R. J.; Bayati, A.; Taft-Benz, S. A.; Smith, J. L.; Wells, C. I.; Madden, E. A.; Brown, J. W.; Lenarcic, E. M.; Yount, B. L., Jr.; Chang, E.; Axtman, A. D.; Baric, R. S.; Heise, M. T.; McPherson, P. S.; Moorman, N. J.; Willson, T. M. Host Kinase CSNK2 is a Target for Inhibition of Pathogenic SARS-like β-Coronaviruses. *ACS Chem. Biol.* **2022**, *17*, 1937−1950.
(29) Cicenas, J.; Zalyte, E.; Bairoch, A.; Gaudet, P. Kinases and Cancer. *Cancers* **2018**, *10*, 63.
(30) Gralinski, L. E.; Baric, R. S. Molecular pathology of emerging coronavirus infections. *J. Pathol.* **2015**, *235*, 185−195.
(31) Davidson, A. D.; Williamson, M. K.; Lewis, S.; Shoemark, D.; Carroll, M. W.; Heesom, K. J.; Zambon, M.; Ellis, J.; Lewis, P. A.; Hiscox, J. A.; Matthews, D. A. Characterisation of the transcriptome and proteome of SARS-CoV-2 reveals a cell passage induced in-frame deletion of the furin-like cleavage site from the spike glycoprotein. *Genome Med.* **2020**, *12*, 68.
(32) Supekar, N. T.; Shajahan, A.; Gleinich, A. S.; Rouhani, D. S.; Heiss, C.; Chapla, D. G.; Moremen, K. W.; Azadi, P. Variable posttranslational modifications of severe acute respiratory syndrome coronavirus 2 nucleocapsid protein. *Glycobiology* **2021**, *31*, 1080−1092.
(33) Gordon, D. E.; Jang, G. M.; Bouhaddou, M.; Xu, J.; Obernier, K.; White, K. M.; O'Meara, M. J.; Rezelj, V. V.; Guo, J. Z.; Swaney, D. L.; Tummino, T. A.; Hüttenhain, R.; Kaake, R. M.; Richards, A. L.; Tutuncuoglu, B.; Foussard, H.; Batra, J.; Haas, K.; Modak, M.; Kim, M.; Haas, P.; Polacco, B. J.; Braberg, H.; Fabius, J. M.; Eckhardt, M.; Soucheray, M.; Bennett, M. J.; Cakir, M.; McGregor, M. J.; Li, Q.; Meyer, B.; Roesch, F.; Vallet, T.; Mac Kain, A.; Miorin, L.; Moreno, E.; Naing, Z. Z. C.; Zhou, Y.; Peng, S.; Shi, Y.; Zhang, Z.; Shen, W.; Kirby, I. T.; Melnyk, J. E.; Chorba, J. S.; Lou, K.; Dai, S. A.; Barrio-Hernandez, I.; Memon, D.; Hernandez-Armenta, C.; Lyu, J.; Mathy,

C. J. P.; Perica, T.; Pilla, K. B.; Ganesan, S. J.; Saltzberg, D. J.; Rakesh, R.; Liu, X.; Rosenthal, S. B.; Calviello, L.; Venkataramanan, S.; Liboy-Lugo, J.; Lin, Y.; Huang, X.-P.; Liu, Y.; Wankowicz, S. A.; Bohn, M.; Safari, M.; Ugur, F. S.; Koh, C.; Savar, N. S.; Tran, Q. D.; Shengjuler, D.; Fletcher, S. J.; O'Neal, M. C.; Cai, Y.; Chang, J. C. J.; Broadhurst, D. J.; Klippsten, S.; Sharp, P. P.; Wenzell, N. A.; Kuzuoglu-Ozturk, D.; Wang, H. Y.; Trenker, R.; Young, J. M.; Cavero, D. A.; Hiatt, J.; Roth, T. L.; Rathore, U.; Subramanian, A.; Noack, J.; Hubert, M.; Stroud, R. M.; Frankel, A. D.; Rosenberg, O. S.; Verba, K. A.; Agard, D. A.; Ott, M.; Emerman, M.; Jura, N.; von Zastrow, M.; Verdin, E.; Ashworth, A.; Schwartz, O.; d'Enfert, C.; Mukherjee, S.; Jacobson, M.; Malik, H. S.; Fujimori, D. G.; Ideker, T.; Craik, C. S.; Floor, S. N.; Fraser, J. S.; Gross, J. D.; Sali, A.; Roth, B. L.; Ruggero, D.; Taunton, J.; Kortemme, T.; Beltrao, P.; Vignuzzi, M.; García-Sastre, A.; Shokat, K. M.; Shoichet, B. K.; Krogan, N. J. A SARS-CoV-2 protein interaction map reveals targets for drug repurposing. *Nature* **2020**, *583*, 459−468.

(34) Attwood, M. M.; Fabbro, D.; Sokolov, A. V.; Knapp, S.; Schiöth, H. B. Trends in kinase drug discovery: targets, indications and inhibitor design. *Nat. Rev. Drug. Discov.* **2021**, *20*, 839−861.

(35) Klaeger, S.; Heinzlmeir, S.; Wilhelm, M.; Polzer, H.; Vick, B.; Koenig, P.-A.; Reinecke, M.; Ruprecht, B.; Petzoldt, S.; Meng, C.; Zecha, J.; Reiter, K.; Qiao, H.; Helm, D.; Koch, H.; Schoof, M.; Canevari, G.; Casale, E.; Re Depaolini, S.; Feuchtinger, A.; Wu, Z.; Schmidt, T.; Rueckert, L.; Becker, W.; Huenges, J.; Garz, A.-K.; Gohlke, B.-O.; Zolg, D. P.; Kayser, G.; Vooder, T.; Preissner, R.; Hahne, H.; Tõnisson, N.; Kramer, K.; Götze, K.; Bassermann, F.; Schlegl, J.; Ehrlich, H.-C.; Aiche, S.; Walch, A.; Greif, P. A.; Schneider, S.; Felder, E. R.; Ruland, J.; Médard, G.; Jeremias, I.; Spiekermann, K.; Kuster, B. The target landscape of clinical kinase drugs. *Science* **2017**, *358*, No. eaan4368.

(36) Sims, A. C.; Burkett, S. E.; Yount, B.; Pickles, R. J. SARS-CoV replication and pathogenesis in an in vitro model of the human conducting airway epithelium. *Virus Res.* **2008**, *133*, 33−44.

(37) Scobey, T.; Yount, B. L.; Sims, A. C.; Donaldson, E. F.; Agnihothram, S. S.; Menachery, V. D.; Graham, R. L.; Swanstrom, J.; Bove, P. F.; Kim, J. D.; Grego, S.; Randell, S. H.; Baric, R. S. Reverse genetics with a full-length infectious cDNA of the Middle East respiratory syndrome coronavirus. *Proc. Natl. Acad. Sci. U. S. A.* **2013**, *110*, 16157−16162.

(38) Hou, Y. J.; Chiba, S.; Halfmann, P.; Ehre, C.; Kuroda, M.; Dinnon, K. H., III; Leist, S. R.; Schäfer, A.; Nakajima, N.; Takahashi, K.; Lee, R. E.; Mascenik, T. M.; Graham, R.; Edwards, C. E.; Tse, L. V.; Okuda, K.; Markmann, A. J.; Bartelt, L.; de Silva, A.; Margolis, D. M.; Boucher, R. C.; Randell, S. H.; Suzuki, T.; Gralinski, L. E.; Kawaoka, Y.; Baric, R. S. SARS-CoV-2 D614G variant exhibits efficient replication ex vivo and transmission in vivo. *Science* **2020**, *370*, 1464−1468.

(39) Hou, Y. J.; Okuda, K.; Edwards, C. E.; Martinez, D. R.; Asakura, T.; Dinnon, K. H., III; Kato, T.; Lee, R. E.; Yount, B. L.; Mascenik, T. M.; Chen, G.; Olivier, K. N.; Ghio, A.; Tse, L. V.; Leist, S. R.; Gralinski, L. E.; Schäfer, A.; Dang, H.; Gilmore, R.; Nakano, S.; Sun, L.; Fulcher, M. L.; Livraghi-Butrico, A.; Nicely, N. I.; Cameron, M.; Cameron, C.; Kelvin, D. J.; de Silva, A.; Margolis, D. M.; Markmann, A.; Bartelt, L.; Zumwalt, R.; Martinez, F. J.; Salvatore, S. P.; Borczuk, A.; Tata, P. R.; Sontake, V.; Kimple, A.; Jaspers, I.; O'Neal, W. K.; Randell, S. H.; Boucher, R. C.; Baric, R. S. SARS-CoV-2 Reverse Genetics Reveals a Variable Infection Gradient in the Respiratory Tract. *Cell* **2020**, *182*, 429−446.e14.

(40) Arend, K. C.; Lenarcic, E. M.; Vincent, H. A.; Rashid, N.; Lazear, E.; McDonald, I. M.; Gilbert, T. S. K.; East, M. P.; Herring, L. E.; Johnson, G. L.; Graves, L. M.; Moorman, N. J. Kinome Profiling Identifies Druggable Targets for Novel Human Cytomegalovirus (HCMV) Antivirals. *Mol. Cell. Proteomics* **2017**, *16*, S263−S276.

(41) Mertins, P.; Tang, L. C.; Krug, K.; Clark, D. J.; Gritsenko, M. A.; Chen, L.; Clauser, K. R.; Clauss, T. R.; Shah, P.; Gillette, M. A.; Petyuk, V. A.; Thomas, S. N.; Mani, D. R.; Mundt, F.; Moore, R. J.; Hu, Y.; Zhao, R.; Schnaubelt, M.; Keshishian, H.; Monroe, M. E.; Zhang, Z.; Udeshi, N. D.; Mani, D.; Davies, S. R.; Townsend, R. R.; Chan, D. W.; Smith, R. D.; Zhang, H.; Liu, T.; Carr, S. A. Reproducible workflow for multiplexed deep-scale proteome and phosphoproteome analysis of tumor tissues by liquid chromatography-mass spectrometry. *Nat. Protoc.* **2018**, *13*, 1632−1661.

(42) McAlister, G. C.; Nusinow, D. P.; Jedrychowski, M. P.; Wühr, M.; Huttlin, E. L.; Erickson, B. K.; Rad, R.; Haas, W.; Gygi, S. P. MultiNotch MS3 enables accurate, sensitive, and multiplexed detection of differential expression across cancer cell line proteomes. *Anal. Chem.* **2014**, *86*, 7150−7158.

(43) Hogrebe, A.; von Stechow, L.; Bekker-Jensen, D. B.; Weinert, B. T.; Kelstrup, C. D.; Olsen, J. V. Benchmarking common quantification strategies for large-scale phosphoproteomics. *Nat. Commun.* **2018**, *9*, 1045.

(44) Tyanova, S.; Temu, T.; Sinitcyn, P.; Carlson, A.; Hein, M. Y.; Geiger, T.; Mann, M.; Cox, J. The Perseus computational platform for comprehensive analysis of (prote)omics data. *Nat. Methods* **2016**, *13*, 731−740.

(45) Hojsgaard, S.; Halekoh, U. *doBy: Gropuwise Statistics, LSmeans, Linear Estimates, Utilities.* **2022**.

(46) Inc., Q. *IPA*, 2022.

(47) Wickham, H.; Averick, M.; Bryan, J.; Chang, W.; McGowan, L. D.'. A.; François, R.; Grolemund, G.; Hayes, A.; Henry, L.; Hester, J.; Kuhn, M.; Pedersen, T. L.; Miller, E.; Bache, S. M.; Müller, K.; Ooms, J.; Robinson, D.; Seidel, D. P.; Spinu, V.; Takahashi, K.; Vaughan, D.; Wilke, C.; Woo, K.; Yutani, H. Welcome to the Tidyverse. *J. Open Source Software* **2019**, *4*, 1686.

(48) Narowski, T. M.; Raphel, K.; Adams, L. E.; Huang, J.; Vielot, N. A.; Jadi, R.; de Silva, A. M.; Baric, R. S.; Lafleur, J. E.; Premkumar, L. SARS-CoV-2 mRNA vaccine induces robust specific and cross-reactive IgG and unequal neutralizing antibodies in naive and previously infected people. *Cell Rep.* **2022**, *38*, No. 110336.

(49) Wells, C. I.; Al-Ali, H.; Andrews, D. M.; Asquith, C. R. M.; Axtman, A. D.; Dikic, I.; Ebner, D.; Ettmayer, P.; Fischer, C.; Frederiksen, M.; Futrell, R. E.; Gray, N. S.; Hatch, S. B.; Knapp, S.; Lücking, U.; Michaelides, M.; Mills, C. E.; Müller, S.; Owen, D.; Picado, A.; Saikatendu, K. S.; Schröder, M.; Stolz, A.; Tellechea, M.; Turunen, B. J.; Vilar, S.; Wang, J.; Zuercher, W. J.; Willson, T. M.; Drewry, D. H. The Kinase Chemogenomic Set (KCGS): An Open Science Resource for Kinase Vulnerability Identification. *Int. J. Mol. Sci.* **2021**, *22*, 566.

(50) Sheahan, T. P.; Sims, A. C.; Leist, S. R.; Schäfer, A.; Won, J.; Brown, A. J.; Montgomery, S. A.; Hogg, A.; Babusis, D.; Clarke, M. O.; Spahn, J. E.; Bauer, L.; Sellers, S.; Porter, D.; Feng, J. Y.; Cihlar, T.; Jordan, R.; Denison, M. R.; Baric, R. S. Comparative therapeutic efficacy of remdesivir and combination lopinavir, ritonavir, and interferon beta against MERS-CoV. *Nat. Commun.* **2020**, *11*, 222.

(51) Dinnon, K. H., III; Leist, S. R.; Schäfer, A.; Edwards, C. E.; Martinez, D. R.; Montgomery, S. A.; West, A.; Yount, B. L., Jr.; Hou, Y. J.; Adams, L. E.; Gully, K. L.; Brown, A. J.; Huang, E.; Bryant, M. D.; Choong, I. C.; Glenn, J. S.; Gralinski, L. E.; Sheahan, T. P.; Baric, R. S. A mouse-adapted model of SARS-CoV-2 to test COVID-19 countermeasures. *Nature* **2020**, *586*, 560−566.

(52) Roskoski, R., Jr. *There are 72 FDA-approved small molecule protein kinase inhibitors.* http://www.brimr.org/PKI/PKIs.htm (accessed October).

(53) Sarwar, M.; Syed Khaja, A. S.; Aleskandarany, M.; Karlsson, R.; Althobiti, M.; Ødum, N.; Mongan, N. P.; Dizeyi, N.; Johnson, H.; Green, A. R.; Ellis, I. O.; Rakha, E. A.; Persson, J. L. The role of PIP5K1α/pAKT and targeted inhibition of growth of subtypes of breast cancer using PIP5K1α inhibitor. *Oncogene* **2019**, *38*, 375−389.

(54) Austin, W. R.; Armijo, A. L.; Campbell, D. O.; Singh, A. S.; Hsieh, T.; Nathanson, D.; Herschman, H. R.; Phelps, M. E.; Witte, O. N.; Czernin, J.; Radu, C. G. Nucleoside salvage pathway kinases regulate hematopoiesis by linking nucleotide metabolism with replication stress. *J. Exp. Med.* **2012**, *209*, 2215−2228.

(55) Guard, S. E.; Poss, Z. C.; Ebmeier, C. C.; Pagratis, M.; Simpson, H.; Taatjes, D. J.; Old, W. M. The nuclear interactome of DYRK1A reveals a functional role in DNA damage repair. *Sci. Rep.* **2019**, *9*, 6539.

(56) Kamitani, W.; Narayanan, K.; Huang, C.; Lokugamage, K.; Ikegami, T.; Ito, N.; Kubo, H.; Makino, S. Severe acute respiratory syndrome coronavirus nsp1 protein suppresses host gene expression by promoting host mRNA degradation. *Proc. Natl. Acad. Sci. U. S. A.* **2006**, *103*, 12885−12890.
(57) Vora, S. M.; Fontana, P.; Mao, T.; Leger, V.; Zhang, Y.; Fu, T. M.; Lieberman, J.; Gehrke, L.; Shi, M.; Wang, L.; Iwasaki, A.; Wu, H. Targeting stem-loop 1 of the SARS-CoV-2 5' UTR to suppress viral translation and Nsp1 evasion. *Proc. Natl. Acad. Sci. U. S. A.* **2022**, *119*, No. e2117198119.
(58) Stukalov, A.; Girault, V.; Grass, V.; Karayel, O.; Bergant, V.; Urban, C.; Haas, D. A.; Huang, Y.; Oubraham, L.; Wang, A.; Hamad, M. S.; Piras, A.; Hansen, F. M.; Tanzer, M. C.; Paron, I.; Zinzula, L.; Engleitner, T.; Reinecke, M.; Lavacca, T. M.; Ehmann, R.; Wölfel, R.; Jöres, J.; Kuster, B.; Protzer, U.; Rad, R.; Ziebuhr, J.; Thiel, V.; Scaturro, P.; Mann, M.; Pichlmair, A. Multilevel proteomics reveals host perturbations by SARS-CoV-2 and SARS-CoV. *Nature* **2021**, *594*, 246−252.
(59) Ragab, D.; Salah Eldin, H.; Taeimah, M.; Khattab, R.; Salem, R. The COVID-19 Cytokine Storm; What We Know So Far. *Front. Immunol.* **2020**, *11*, 1446.
(60) Lin, L.; Shao, J.; Sun, M.; Liu, J.; Xu, G.; Zhang, X.; Xu, N.; Wang, R.; Liu, S. Identification of phosphorylation sites in the nucleocapsid protein (N protein) of SARS-coronavirus. *Int. J. Mass Spectrom.* **2007**, *268*, 296−303.
(61) Dang, M.; Li, Y.; Song, J. ATP biphasically modulates LLPS of SARS-CoV-2 nucleocapsid protein and specifically binds its RNA-binding domain. *Biochem. Biophys. Res. Commun.* **2021**, *541*, 50−55.
(62) Dang, M.; Song, J. CTD of SARS-CoV-2 N protein is a cryptic domain for binding ATP and nucleic acid that interplay in modulating phase separation. *Protein Sci.* **2022**, *31*, 345−356.
(63) Sheahan, T. P.; Sims, A. C.; Graham, R. L.; Menachery, V. D.; Gralinski, L. E.; Case, J. B.; Leist, S. R.; Pyrc, K.; Feng, J. Y.; Trantcheva, I.; Bannister, R.; Park, Y.; Babusis, D.; Clarke, M. O.; Mackman, R. L.; Spahn, J. E.; Palmiotti, C. A.; Siegel, D.; Ray, A. S.; Cihlar, T.; Jordan, R.; Denison, M. R.; Baric, R. S. Broad-spectrum antiviral GS-5734 inhibits both epidemic and zoonotic coronaviruses. *Sci. Transl. Med.* **2017**, *9*, No. eaal3653.
(64) Brown, A. J.; Won, J. J.; Graham, R. L.; Dinnon, K. H., III; Sims, A. C.; Feng, J. Y.; Cihlar, T.; Denison, M. R.; Baric, R. S.; Sheahan, T. P. Broad spectrum antiviral remdesivir inhibits human endemic and zoonotic deltacoronaviruses with a highly divergent RNA dependent RNA polymerase. *Antiviral Res.* **2019**, *169*, No. 104541.
(65) Cavazzoni, A.; Alfieri, R. R.; Cretella, D.; Saccani, F.; Ampollini, L.; Galetti, M.; Quaini, F.; Graiani, G.; Madeddu, D.; Mozzoni, P.; Galvani, E.; La Monica, S.; Bonelli, M.; Fumarola, C.; Mutti, A.; Carbognani, P.; Tiseo, M.; Barocelli, E.; Petronini, P. G.; Ardizzoni, A. Combined use of anti-ErbB monoclonal antibodies and erlotinib enhances antibody-dependent cellular cytotoxicity of wild-type erlotinib-sensitive NSCLC cell lines. *Mol. Cancer* **2012**, *11*, 91.
(66) Ely, E. W.; Ramanan, A. V.; Kartman, C. E.; de Bono, S.; Liao, R.; Piruzeli, M. L. B.; Goldman, J. D.; Saraiva, J. F. K.; Chakladar, S.; Marconi, V. C.; COV - Barrier study Group. Efficacy and safety of baricitinib plus standard of care for the treatment of critically ill hospitalised adults with COVID-19 on invasive mechanical ventilation or extracorporeal membrane oxygenation: an exploratory, randomised, placebo-controlled trial. *Lancet Respir. Med.* **2022**, *10*, 327−336.
(67) Roschewski, M.; Lionakis, M. S.; Sharman, J. P.; Roswarski, J.; Goy, A.; Monticelli, M. A.; Roshon, M.; Wrzesinski, S. H.; Desai, J. V.; Zarakas, M. A.; Collen, J.; Rose, K. M.; Hamdy, A.; Izumi, R.; Wright, G. W.; Chung, K. K.; Baselga, J.; Staudt, L. M.; Wilson, W. H. Inhibition of Bruton tyrosine kinase in patients with severe COVID-19. *Sci. Immunol.* **2020**, *5*, No. eabd0110.
(68) Singh, P.; Behera, D.; Gupta, S.; Deep, A.; Priyadarshini, S.; Padhan, P. Nintedanib vs pirfenidone in the management of COVID-19 lung fibrosis: A single-centre study. *J. R. Coll. Physicians Edinburgh* **2022**, *52*, 100−104.
(69) Baric, R. S.; Nelson, G. W.; Fleming, J. O.; Deans, R. J.; Keck, J. G.; Casteel, N.; Stohlman, S. A. Interactions between coronavirus nucleocapsid protein and viral RNAs: implications for viral transcription. *J. Virol.* **1988**, *62*, 4280−4287.
(70) Narayanan, K.; Kim, K. H.; Makino, S. Characterization of N protein self-association in coronavirus ribonucleoprotein complexes. *Virus Res.* **2003**, *98*, 131−140.
(71) Savastano, A.; Ibáñez de Opakua, A.; Rankovic, M.; Zweckstetter, M. Nucleocapsid protein of SARS-CoV-2 phase separates into RNA-rich polymerase-containing condensates. *Nat. Commun.* **2020**, *11*, 6041.
(72) Lang, Y.; Chen, K.; Li, Z.; Li, H. The nucleocapsid protein of zoonotic betacoronaviruses is an attractive target for antiviral drug discovery. *Life Sci.* **2021**, *282*, 118754.
(73) Zúñiga, S.; Cruz, J. L. G.; Sola, I.; Mateos-Gómez, P. A.; Palacio, L.; Enjuanes, L. Coronavirus nucleocapsid protein facilitates template switching and is required for efficient transcription. *J. Virol.* **2010**, *84*, 2169−2175.
(74) Wang, Z. N.; Yang, X. S.; Sun, J.; Zhao, J. C.; Zhong, N. S.; Tang, X. X. Multi-omics evaluation of SARS-CoV-2 infected mouse lungs reveals dynamics of host responses. *iScience* **2022**, *25*, No. 103967.
(75) Cantwell, A. M.; Singh, H.; Platt, M.; Yu, Y.; Lin, Y. H.; Ikeno, Y.; Hubbard, G.; Xiang, Y.; Gonzalez-Juarbe, N.; Dube, P. H. Kinetic Multi-omic Analysis of Responses to SARS-CoV-2 Infection in a Model of Severe COVID-19. *J. Virol.* **2021**, *95*, No. e0101021.
(76) Liu, J. F.; Zhou, Y. N.; Lu, S. Y.; Yang, Y. H.; Wu, S. F.; Liu, D. P.; Peng, X. Z.; Yang, J. T. Proteomic and phosphoproteomic profiling of COVID-19-associated lung and liver injury: a report based on rhesus macaques. *Signal Transduction Targeted Ther.* **2022**, *7*, 27.
(77) Vanderboom, P. M.; Mun, D. G.; Madugundu, A. K.; Mangalaparthi, K. K.; Saraswat, M.; Garapati, K.; Chakraborty, R.; Ebihara, H.; Sun, J.; Pandey, A. Proteomic Signature of Host Response to SARS-CoV-2 Infection in the Nasopharynx. *Mol. Cell. Proteomics* **2021**, *20*, No. 100134.
(78) Appelberg, S.; Gupta, S.; Svensson Akusjärvi, S.; Ambikan, A. T.; Mikaeloff, F.; Saccon, E.; Végvári, Á.; Benfeitas, R.; Sperk, M.; Ståhlberg, M.; Krishnan, S.; Singh, K.; Penninger, J. M.; Mirazimi, A.; Neogi, U. Dysregulation in Akt/mTOR/HIF-1 signaling identified by proteo-transcriptomics of SARS-CoV-2 infected cells. *Emerging Microbes Infect.* **2020**, *9*, 1748−1760.
(79) Kindrachuk, J.; Ork, B.; Hart, B. J.; Mazur, S.; Holbrook, M. R.; Frieman, M. B.; Traynor, D.; Johnson, R. F.; Dyall, J.; Kuhn, J. H.; Olinger, G. G.; Hensley, L. E.; Jahrling, P. B. Antiviral potential of ERK/MAPK and PI3K/AKT/mTOR signaling modulation for Middle East respiratory syndrome coronavirus infection as identified by temporal kinome analysis. *Antimicrob. Agents Chemother.* **2015**, *59*, 1088−1099.
(80) Pan, C.; Kumar, C.; Bohl, S.; Klingmueller, U.; Mann, M. Comparative proteomic phenotyping of cell lines and primary cells to assess preservation of cell type-specific functions. *Mol. Cell. Proteomics* **2009**, *8*, 443−450.
(81) Alge, C. S.; Hauck, S. M.; Priglinger, S. G.; Kampik, A.; Ueffing, M. Differential protein profiling of primary versus immortalized human RPE cells identifies expression patterns associated with cytoskeletal remodeling and cell survival. *J. Proteome Res.* **2006**, *5*, 862−878.
(82) Garcia, G., Jr.; Sharma, A.; Ramaiah, A.; Sen, C.; Purkayastha, A.; Kohn, D. B.; Parcells, M. S.; Beck, S.; Kim, H.; Bakowski, M. A.; Kirkpatrick, M. G.; Riva, L.; Wolff, K. C.; Han, B.; Yuen, C.; Ulmert, D.; Purbey, P. K.; Scumpia, P.; Beutler, N.; Rogers, T. F.; Chatterjee, A. K.; Gabriel, G.; Bartenschlager, R.; Gomperts, B.; Svendsen, C. N.; Betz, U. A. K.; Damoiseaux, R. D.; Arumugaswami, V. Antiviral drug screen identifies DNA-damage response inhibitor as potent blocker of SARS-CoV-2 replication. *Cell Rep.* **2021**, *35*, No. 108940.
(83) Weisberg, E.; Parent, A.; Yang, P. L.; Sattler, M.; Liu, Q.; Liu, Q.; Wang, J.; Meng, C.; Buhrlage, S. J.; Gray, N.; Griffin, J. D. Repurposing of Kinase Inhibitors for Treatment of COVID-19. *Pharm. Res.* **2020**, *37*, 167.

(84) Acharya, A.; Pathania, A. S.; Pandey, K.; Thurman, M.; Vann, K. R.; Kutateladze, T. G.; Challagundala, K. B.; Durden, D. L.; Byrareddy, S. N. PI3K- α /mTOR/BRD4 inhibitor alone or in combination with other anti-virals blocks replication of SARS-CoV-2 and its variants of concern including Delta and Omicron. *Clin. Transl. Med.* **2022**, *12*, No. e806.
(85) Logue, J.; Chakraborty, A. R.; Johnson, R.; Goyal, G.; Rodas, M.; Taylor, L. J.; Baracco, L.; McGrath, M. E.; Haupt, R.; Furlong, B. A.; Soong, M.; Prabhala, P.; Horvath, V.; Carlson, K. E.; Weston, S.; Ingber, D. E.; DePamphilis, M. L.; Frieman, M. B. PIKfyve-specific inhibitors restrict replication of multiple coronaviruses in vitro but not in a murine model of COVID-19. *Commun. Biol.* **2022**, *5*, 808.
(86) Edwards, C. E.; Tata, A.; Baric, R. S. Human lung organoids as a model for respiratory virus replication and countermeasure performance in human hosts. *Transl. Res.* **2022**, 36.
(87) Kong, N.; Wu, Y.; Meng, Q.; Wang, Z.; Zuo, Y.; Pan, X.; Tong, W.; Zheng, H.; Li, G.; Yang, S.; Yu, H.; Zhou, E. M.; Shan, T.; Tong, G. Suppression of Virulent Porcine Epidemic Diarrhea Virus Proliferation by the PI3K/Akt/GSK-3α/β Pathway. *PLoS One* **2016**, *11*, No. e0161508.
(88) Lin, H.; Li, B.; Liu, M.; Zhou, H.; He, K.; Fan, H. Nonstructural protein 6 of porcine epidemic diarrhea virus induces autophagy to promote viral replication via the PI3K/Akt/mTOR axis. *Vet. Microbiol.* **2020**, *244*, No. 108684.
(89) Liu, G. Y.; Sabatini, D. M. mTOR at the nexus of nutrition, growth, ageing and disease. *Nat. Rev. Mol. Cell Biol.* **2020**, *21*, 183−203.
(90) Mizutani, T.; Fukushi, S.; Ishii, K.; Sasaki, Y.; Kenri, T.; Saijo, M.; Kanaji, Y.; Shirota, K.; Kurane, I.; Morikawa, S. Mechanisms of establishment of persistent SARS-CoV-infected cells. *Biochem. Biophys. Res. Commun.* **2006**, *347*, 261−265.
(91) Fujioka, Y.; Tsuda, M.; Hattori, T.; Sasaki, J.; Sasaki, T.; Miyazaki, T.; Ohba, Y. The Ras-PI3K signaling pathway is involved in clathrin-independent endocytosis and the internalization of influenza viruses. *PLoS One* **2011**, *6*, No. e16324.
(92) Khezri, M. R.; Varzandeh, R.; Ghasemnejad-Berenji, M. The probable role and therapeutic potential of the PI3K/AKT signaling pathway in SARS-CoV-2 induced coagulopathy. *Cell Mol. Biol. Lett.* **2022**, *27*, 6.
(93) Richardson, P.; Griffin, I.; Tucker, C.; Smith, D.; Oechsle, O.; Phelan, A.; Rawling, M.; Savory, E.; Stebbing, J. Baricitinib as potential treatment for 2019-nCoV acute respiratory disease. *Lancet* **2020**, *395*, e30−e31.
(94) Bronte, V.; Ugel, S.; Tinazzi, E.; Vella, A.; De Sanctis, F.; Canè, S.; Batani, V.; Trovato, R.; Fiore, A.; Petrova, V.; Hofer, F.; Barouni, R. M.; Musiu, C.; Caligola, S.; Pinton, L.; Torroni, L.; Polati, E.; Donadello, K.; Friso, S.; Pizzolo, F.; Iezzi, M.; Facciotti, F.; Pelicci, P. G.; Righetti, D.; Bazzoni, P.; Rampudda, M.; Comel, A.; Mosaner, W.; Lunardi, C.; Olivieri, O. Baricitinib restrains the immune dysregulation in patients with severe COVID-19. *J. Clin. Invest.* **2020**, *130*, 6409−6416.
(95) Horie, S.; McNicholas, B.; Rezoagli, E.; Pham, T.; Curley, G.; McAuley, D.; O'Kane, C.; Nichol, A.; Dos Santos, C.; Rocco, P. R. M.; Bellani, G.; Laffey, J. G. Emerging pharmacological therapies for ARDS: COVID-19 and beyond. *Intensive Care Med.* **2020**, *46*, 2265−2283.
(96) Oliveira, G. P.; Silva, J. D.; Marques, P. S.; Gonçalves-de-Albuquerque, C. F.; Santos, H. L.; Vascocellos, A. P.; Takiya, C. M.; Morales, M. M.; Pelosi, P.; Mócsai, A.; de Castro-Faria-Neto, H. C.; Rocco, P. R. M. The Effects of Dasatinib in Experimental Acute Respiratory Distress Syndrome Depend on Dose and Etiology. *Cell. Physiol. Biochem.* **2015**, *36*, 1644−1658.
(97) Rizzo, A. N.; Sammani, S.; Esquinca, A. E.; Jacobson, J. R.; Garcia, J. G. N.; Letsiou, E.; Dudek, S. M. Imatinib attenuates inflammation and vascular leak in a clinically relevant two-hit model of acute lung injury. *Am. J. Physiol. Lung Cell Mol. Physiol.* **2015**, *309*, L1294−L1304.
(98) Strich, J. R.; Tian, X.; Samour, M.; King, C. S.; Shlobin, O.; Reger, R.; Cohen, J.; Ahmad, K.; Brown, A. W.; Khangoora, V.; Aryal, S.; Migdady, Y.; Kyte, J. J.; Joo, J.; Hays, R.; Collins, A. C.; Battle, E.; Valdez, J.; Rivero, J.; Kim, I. K.; Erb-Alvarez, J.; Shalhoub, R.; Chakraborty, M.; Wong, S.; Colton, B.; Ramos-Benitez, M. J.; Warner, S.; Chertow, D. S.; Olivier, K. N.; Aue, G.; Davey, R. T.; Suffredini, A. F.; Childs, R. W.; Nathan, S. D. Fostamatinib for the treatment of hospitalized adults with Coronavirus Disease 2019: A randomized trial. *Clin. Infect. Dis.* **2022**, *75*, e491−e498.
(99) Apostolidis, S. A.; Sarkar, A.; Giannini, H. M.; Goel, R. R.; Mathew, D.; Suzuki, A.; Baxter, A. E.; Greenplate, A. R.; Alanio, C.; Abdel-Hakeem, M.; Oldridge, D. A.; Giles, J. R.; Wu, J. E.; Chen, Z.; Huang, Y. J.; Belman, J.; Pattekar, A.; Manne, S.; Kuthuru, O.; Dougherty, J.; Weiderhold, B.; Weisman, A. R.; Ittner, C. A. G.; Gouma, S.; Dunbar, D.; Frank, I.; Huang, A. C.; Vella, L. A.; The UPenn COVID Processing Unit; Reilly, J. P.; Hensley, S. E.; Rauova, L.; Zhao, L.; Meyer, N. J.; Poncz, M.; Abrams, C. S.; Wherry, E. J. Signaling Through FcγRIIA and the C_5a-C_5aR Pathway Mediate Platelet Hyperactivation in COVID-19. *Front. Immunol.* **2022**, *13*, No. 834988.
(100) Kost-Alimova, M.; Sidhom, E. H.; Satyam, A.; Chamberlain, B. T.; Dvela-Levitt, M.; Melanson, M.; Alper, S. L.; Santos, J.; Gutierrez, J.; Subramanian, A.; Byrne, P. J.; Grinkevich, E.; Reyes-Bricio, E.; Kim, C.; Clark, A. R.; Watts, A. J. B.; Thompson, R.; Marshall, J.; Pablo, J. L.; Coraor, J.; Roignot, J.; Vernon, K. A.; Keller, K.; Campbell, A.; Emani, M.; Racette, M.; Bazua-Valenti, S.; Padovano, V.; Weins, A.; McAdoo, S. P.; Tam, F. W. K.; Ronco, L.; Wagner, F.; Tsokos, G. C.; Shaw, J. L.; Greka, A. A High-Content Screen for Mucin-1-Reducing Compounds Identifies Fostamatinib as a Candidate for Rapid Repurposing for Acute Lung Injury. *Cell Rep. Med.* **2020**, *1*, No. 100137.
(101) Sims, A. C.; Mitchell, H. D.; Gralinski, L. E.; Kyle, J. E.; Burnum-Johnson, K. E.; Lam, M.; Fulcher, M. L.; West, A.; Smith, R. D.; Randell, S. H.; Metz, T. O.; Sheahan, T. P.; Waters, K. M.; Baric, R. S. Unfolded Protein Response Inhibition Reduces Middle East Respiratory Syndrome Coronavirus-Induced Acute Lung Injury. *MBio* **2021**, *12*, No. e0157221.